EUROPEAN ORGANIZATION FOR NUCLEAR RESEARCH (CERN)
FERMILAB-PUB-11-700-CMS

CERN-PH-EP/2011-085
2011/08/19

CMS-TOP-10-003

arXiv:1108.3773v1 [hep-ex] 18 Aug 2011

Measurement of the $t\bar{t}$ Production Cross Section in pp Collisions at 7 TeV in Lepton + Jets Events Using b-quark Jet Identification

The CMS Collaboration*

Abstract

A new measurement of the inclusive production cross section for $pp \to t\bar{t}$ is performed at a center-of-mass energy of 7 TeV using data collected by the CMS experiment at the LHC. The analysis uses a data sample corresponding to an integrated luminosity of $36\,\mathrm{pb}^{-1}$, and is based on the final state with one isolated, high transverse momentum muon or electron, missing transverse energy, and hadronic jets. The $t\bar{t}$ content of the selected events is enhanced by requiring the presence of at least one jet consistent with b-quark hadronization. The measured cross section is 150 ± 9 (stat.) ± 17 (syst.) ± 6 (lumi.) pb and is in agreement with higher-order QCD calculations. The combination of this measurement with a previous CMS result based on dileptons gives 154 ± 17 (stat. + syst.) ± 6 (lumi.) pb.

Submitted to Physical Review D

*See Appendix A for the list of collaboration members

Operated by Fermi Research Alliance, LLC under Contract No. De-AC02-07CH11359 with the United States Department of Energy.

1 Introduction

The top quark was first observed in proton-antiproton collisions at $\sqrt{s} = 1.8$ TeV at the Fermilab Tevatron collider [1, 2]. Since then its properties have been studied by the Tevatron experiments and found to be in agreement with the expectations of the standard model (SM) [3]. At the Large Hadron Collider (LHC) [4] top quark production can be studied in pp collisions at $\sqrt{s}$ = 7 TeV, allowing extended measurements of the top quark properties. A precise measurement of these properties is important as top-quark production may be a background for new physics.

At the LHC top quarks can be produced singly or in pairs. This paper focuses on the study of the $t\bar{t}$ final state, for which the production cross section has been calculated in next-to-leading-order (NLO) and approximate next-to-next-to-leading-order (NNLO) quantum chromodynamics (QCD) [5–7]. In the SM the top quark decays almost 100% of the time via the weak process $t \to Wb$. We focus on the $t\bar{t}$ decays in which one of the two W bosons decays hadronically and the other decays leptonically (the semileptonic channel), giving a final state containing an electron or muon, a neutrino, and four jets, two of which come from the hadronization of b quarks. Here taus are detected only through their semileptonic decays to electrons and muons. The results are based on the analysis of a data sample corresponding to an integrated luminosity of $36\,\mathrm{pb}^{-1}$ [8], which was recorded by the Compact Muon Solenoid (CMS) experiment between April and November 2010.

We present the results of $t\bar{t}$ cross section measurements in the muon and electron + jets channels using the subset of the data in which at least one jet has been b tagged using a displaced secondary vertex algorithm. A profile likelihood method is used to fit the mass distribution of the identified b-decay vertices as a function of the jet and b-tag multiplicities in the event. The analysis is sensitive to the differences between the signal and background processes and also allows the simultaneous fit of the light (u, d, s) and heavy quark (b, c) contributions. The main systematic uncertainties are taken into account when maximizing the profile likelihood. This allows for the correct treatment of their correlations and the evaluation of the combined uncertainty. These results complement the CMS dilepton and kinematics-based lepton+jets analyses which are described elsewhere [9, 10]. The ATLAS experiment has also measured the $t\bar{t}$ cross section in the dilepton and lepton+jets channels at 7 TeV [11]. Several cross-check analyses are also performed, which use different analysis techniques (a fit without the use of the profile likelihood, and two measurements based on simple cuts), and different b-tag algorithms (one based on a track impact parameter, and another that uses soft muons).

The central feature of the CMS detector is a superconducting solenoid, 13 m in length and 6 m in diameter, which provides an axial magnetic field of 3.8 T. The inside of the solenoid is outfitted with various particle detection systems. Charged particle trajectories are measured by the silicon pixel and strip tracker, covering $0 < \phi < 2\pi$ in azimuth and $|\eta| < 2.5$, where the pseudorapidity η is defined as $\eta = -\ln[\tan(\theta/2)]$, and θ is the polar angle of the trajectory with respect to the anti-clockwise beam direction. A crystal calorimeter and a brass/scintillator calorimeter surround the tracking volume and provide high resolution energy and direction measurements of electrons, photons, and hadronic jets. Muons are measured in gas-ionization detectors embedded in the steel return yoke outside the solenoid. The detector is nearly hermetic, allowing for energy balance measurements in the plane transverse to the beam direction. A two-tier trigger system selects the most interesting pp collision events for use in physics analysis. A more detailed description of the CMS detector can be found elsewhere [12].

We describe the data and event selection in Section 2 of this paper, followed by a brief description of the modeling of the signal and background processes in Section 3. Section 4 describes the method used to extract the cross section from the selected events, as well as the calculation

of the statistical and systematic uncertainties on the result. The cross-check analyses are discussed briefly in Section 5. Lastly, in Sections 6 and 7 we present a summary of all of the CMS measurements and compare the results with the predictions from QCD.

2 Event Selection

The trigger used to select the data samples for analysis is based on the presence of at least one charged lepton, with either an electron or a muon with a transverse momentum, $p_T > p_T^{min}$. Because of increasing maximum instantaneous luminosity, the minimum transverse momentum was varied between 9 and 15 GeV for muons and between 10 and 22 GeV for electrons in order to maintain a reasonable trigger rate. The same data are used both for signal selection and for the study of the non-top QCD multijet and W(Z)+jets backgrounds. These triggers have been shown to have efficiencies of $92.2 \pm 0.2\%$ and $98.2 \pm 0.1\%$ for the muon and electron channels, respectively, based on independent studies of Z boson decays into $\mu^+\mu^-$ and e^+e^- pairs. No azimuthal nor polar angle dependence is observed.

Muons are reconstructed using the information from the muon chambers and the silicon tracker and required to be consistent with the reconstructed primary vertex [13]. A kinematic selection requiring $p_T > 20$ GeV and $|\eta| < 2.1$ is then used to select muon tracks for further analysis. Electrons are reconstructed using a combination of shower shape information and track/electromagnetic-cluster matching [14]. A veto is applied to reject the electrons coming from photon conversions. To be retained for further analysis, electron candidates are required to have a transverse energy, $E_T > 30$ GeV and $|\eta| < 2.5$, excluding the transition region between the barrel and endcap calorimeters, $1.44 < |\eta_c| < 1.57$, where η_c is the pseudorapidity of the electromagnetic cluster.

Signal events are required to have only one isolated lepton, whose origin is consistent with the reconstructed pp interaction vertex [15]. Since the muon (electron) from a leptonic W decay is expected to be isolated from other high-p_T particles in the event, its track is required to be isolated from other activity in the event. This is done by requiring a relative isolation (I_{rel}) less than 0.05 for muons and 0.10 for electrons. A looser cut is used in the electron case to allow for the increased amount of radiation close to the track. Relative isolation is defined as $I_{rel} = (I_{charged} + I_{neutral} + I_{photon})/p_T$, where p_T is the transverse momentum of the lepton, and $I_{charged}$, $I_{neutral}$, and I_{photon} are the sums of the transverse energies of the charged and neutral hadrons and the photons reconstructed in a cone of $\Delta R < 0.3$ around the lepton direction, where $\Delta R = \sqrt{(\Delta\phi)^2 + (\Delta\eta)^2}$. The energy deposited by the lepton is explicitly removed from the sums by defining an exclusion cone of $\Delta R < 0.15$ around the lepton direction. From studies based on Z decays in the data, the combined identification and isolation efficiencies for these selections are $83 \pm 1\%$ for muons and $75 \pm 1\%$ for electrons.

Semileptonic $t\bar{t}$ events have at least four hadronic jets (from the hadronization of the bottom and light quarks). Charged and neutral hadrons, photons, and leptons are reconstructed using the CMS particle-flow algorithm [16] before they are clustered to form jets using the anti-k_T jet algorithm [17] with a cone size $\Delta R = 0.5$. The jet clustering software used is FASTJET version 2.4.2 [18, 19]. At least one jet candidate with $p_T > 25$ GeV and $|\eta| < 2.4$ is required, which must not overlap with a muon or electron candidate within $\Delta R < 0.3$. Relative and absolute jet energy corrections [20] are applied to the raw jet momenta to establish a uniform jet response in p_T and η (with uncertainties of 3–6%, dependent on p_T and η). An offset correction, determined from simulation, is made to correct for the effects of event pileup (with an uncertainty $< 1.4\%$). There is an additional b-jet energy scale uncertainty which accounts for the differences in response between PYTHIA and HERWIG simulations ($\sim$3%). Lastly, a further 1.5% uncertainty

is added to allow for residual calibration differences during different run periods for a total of 4.7–7.0%.

The neutrino from the leptonic W decay escapes detection. Its presence is inferred from a sizeable transverse energy imbalance in the detector. The missing transverse energy ($\not{E}_{\mathrm{T}}$) is defined as the negative of the vector sum of the transverse energies (E_{T}) of all of the particles found by the particle-flow algorithm. This is used as an event selection variable in both the muon and electron analyses to suppress the background from QCD multijet events, and is required to be greater than 20 GeV in both channels.

Because of the combined effects of the long b-quark lifetime ($\sim$1.5 ps) and the fact that the b quarks are produced with a significant boost, the decays of b-flavored hadrons are quite different from the shorter lived hadronic states. Rather than having an origin consistent with the primary collision vertex, they can travel a measurable distance before decaying, resulting in a displaced decay vertex. The origin of the particles from the b decay is thus typically inconsistent with the primary vertex position. In the case of a semileptonic b-hadron decay, this results in the production of a lepton with a displaced origin, that is also embedded inside a jet. These characteristics can be used to identify b-quark jets and distinguish them from their non-b counterparts. Here we use a displaced secondary vertex algorithm to tag b decays and suppress the background from W(Z)+jet and QCD multijet events. The algorithm is described in detail in [21] and has a b-tag efficiency of 55% with a light parton (u, d, s, g) mistag rate of 1.5% for jets with $p_{\mathrm{T}} > 30$ GeV in simulated QCD events. The event selection requires that at least one of the selected jets is b tagged.

3 Signal and Background Modeling

The efficiency for selecting lepton+jets signal events and the corresponding kinematic distributions are modeled using a simulated $\mathrm{t\bar{t}}$ event sample. The simulation is performed using MADGRAPH [22], where the events containing top-quark pairs are generated accompanied by up to three extra partons in the matrix-element calculation. The parton configurations generated by MADGRAPH are processed with PYTHIA 6.4 [23] to provide fragmentation of the generated partons. The shower matching is done using the Kt-MLM prescription [22]. The generated events are then passed through the full CMS detector simulation based on GEANT4 [24].

The production of W(Z) + jets events, where the vector boson decays leptonically, has a similar signature and constitutes the main background. These are also simulated using MADGRAPH. We use a dynamical mass scale (Q^2 scale) of $(m_{\mathrm{W/Z}})^2 + (\sum p_{\mathrm{T}}^{\mathrm{jet}})^2$ for the renormalization and factorization scales for both the W+jets and Z+jets simulations, and these scales are varied by factors of 2.0 and 0.5 in systematic studies.

In addition to the Monte Carlo (MC) generation using MADGRAPH, QCD multijet samples were produced using PYTHIA.

The QCD predictions for the top-quark pair production cross section are 157^{+23}_{-24} pb in NLO [25] and 164^{+10}_{-13} pb [5, 6] or 163^{+11}_{-10} pb [7] in approximate NNLO. In each case the quoted uncertainties include the renormalization and factorization scale uncertainties, the uncertainties from the choice of parton distribution functions (PDF)s, and the uncertainty of the strong coupling constant (α_S). For the scale uncertainty we have varied the renormalization and factorization scales by factors of 2 and 0.5 around the central choice of $(2m_{\mathrm{t}})^2 + (\sum p_{\mathrm{T}}^{\mathrm{jet}})^2$ with $m_{\mathrm{t}} = 172.5$ GeV. The PDF and α_S uncertainties were determined by following the results obtained by using the MSTW2008 [26], CTEQ6.6 [27], and NNPDF2.0 [28] sets and combining the results using the

PDF4LHC prescriptions [29].

Single top quark production is described in terms of the cross sections in the s, t and tW channels. The largest cross section is in the t channel where the predicted NLO cross section is $\sigma_t = 64.6^{+3.4}_{-3.2}$ pb from MCFM [25, 30–32]. The result is given for a scale of $(m_t)^2 + (\sum p_T^{jet})^2$ and an uncertainty that is defined in the same way as for top-quark pair production. Similarly, the cross sections for the tW and s channels are predicted to be $\sigma_{tW} = 10.6 \pm 0.8$ pb and $\sigma_s = 4.2 \pm 0.2$ pb [30], respectively. A measurement of the t-channel cross section has been performed by CMS and is found to be consistent with the value predicted by the standard model [33].

The inclusive NNLO cross section of the production of W bosons decaying into leptons has been determined as $\sigma_{W\to l\nu} = 31.3 \pm 1.6$ nb using FEWZ [34] (corresponding to a k-factor of 1.3), setting renormalization and factorization scales to m_W^2 with $m_W = 80.398$ GeV. The uncertainty was determined in a similar way as for top-quark pair production. Finally, the Drell–Yan production cross section at NNLO has been calculated using FEWZ as $\sigma_{Z/\gamma^*\to ll}(m_{ll} > 50\,\text{GeV}) = 3.0 \pm 0.1$ nb where the scales were set to m_Z^2 with $m_Z = 91.1876$ GeV.

The cross sections discussed above are used to normalize the simulated event samples. The profile likelihood fit yields corrections to these values. The normalizations for the final comparisons with the data are determined from fits to the data in control samples.

4 Cross Section Measurements

The following subsections discuss the measurement procedure and the results obtained from the analysis of the muon, electron and combined channels.

4.1 Fit Procedure

To extract the $t\bar{t}$ cross section we perform a maximum likelihood fit to the number of reconstructed jets ($j = 1$–4, $\geq$5), the number of b-tagged jets ($i = 1, \geq 2$), and the secondary vertex mass distribution in the data. The secondary vertex mass is defined as the mass of the sum of the four-vectors of the tracks associated to the secondary vertex, assuming that each particle has the pion mass. It gives a good discrimination between the contributions from light and heavy flavor quark production (Fig. 1). We fit the data to the sum of signal and background shapes using a binned Poisson likelihood.

The templates for the fit are normalized to the expected event yields for 36 pb^{-1}. The expected yield for each component in a given jet-multiplicity bin j and tag-multiplicity bin i is a function of the cross section, the jet energy scale (JES), the b-tag efficiency, and the background normalization. The JES and the Q^2-scales affect the jet multiplicity, and the b-tag efficiency impacts the number of b tags. The background model depends on each of these and has additional contributions from the normalization and extrapolation from the sidebands in the data. Because these effects are expected to cause the largest uncertainties on the $t\bar{t}$ cross section measurement, and they are correlated, they are treated as nuisance parameters in the profile likelihood fit. The minimization of the likelihood thus provides simultaneous measurements of each contribution and the $t\bar{t}$ cross section.

We determine the background normalizations from data sideband regions and extrapolate to the signal region using various models. In particular, the four major backgrounds are W+jets, Z+jets, single top quark, and QCD multijet production.

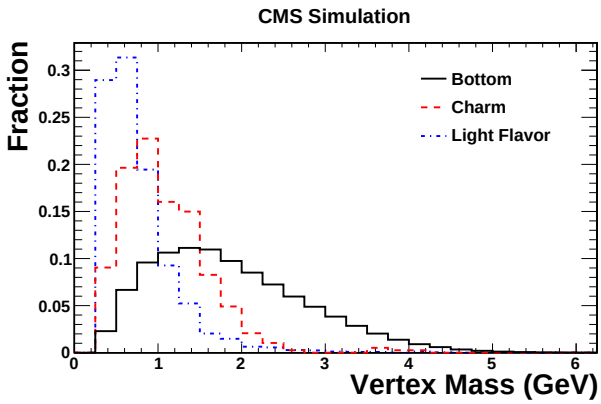

Figure 1: Secondary vertex mass distribution for bottom, charm, and light flavor jets. The bottom and charm templates are taken from simulated $t\bar{t}$ events and the light flavor shape is taken from simulated W+jet events.

The templates for the W and Z contributions are normalized such that the NNLO predictions are equal to unity. During the profile likelihood maximization, the normalizations of these components are extracted. A full detector unfolding is not done, so this is not a meaningful measurement of the $W(Z)$+jets cross section, however the impact of the renormalization and factorization scales on the $t\bar{t}$ cross section is found to be smaller than that predicted by an ad hoc variation of the scales.

The W and $Z+$ jets backgrounds come from V+b jets, V+c jets, and V+light flavor events. The same k-factor of 1.30 (defined in Section 3) is applied to all three flavors as inputs to the likelihood fit (although the three components are allowed to float independently in the fit). An additional electroweak background is single-top (s and t and tW channels) events.

The shape of the jet multiplicity distribution (N_{jet}) depends on the choice of the jet p_{T} threshold, and thus is also sensitive to the jet energy scale (JES). In this sense, the fit is intrinsically able to determine the JES from the variations of the N_{jet} distribution as a function of JES. The uncertainty in the b-tag efficiency is also extracted directly from the fit, by using the changes in the relative rates of 1-tag, and 2-tag events. A larger b-tag efficiency will result in events moving from 1-tag to 2-tag samples. In contrast, an overall increase in all tag bins together would indicate an increase in the $t\bar{t}$ cross section. The combined in-situ measurement of the yields of principal backgrounds and parameters describing main systematic uncertainties leads to a significant improvement over analyses which use more conventional techniques for tagged cross section measurements.

There are several "nonprompt-W" or "QCD" backgrounds for the muon and electron analyses. The QCD background in the muon-plus-jets channel comes from multijet events with heavy flavor decays, kaon and pion decays in flight, and hadronic punch-through in the muon system. Because these are difficult to calculate to the required precision we derive these backgrounds from the data. The normalization is determined by using a comparison of data and simulation in the data sideband region with $\not{E}_{\text{T}} < 20\,\text{GeV}$. The ratio is used to scale the predicted yields for $\not{E}_{\text{T}} > 20\,\text{GeV}$. The shapes and normalizations of the $t\bar{t}$, W and Z+jets are well described by the Monte Carlo simulation and are modeled that way. The shape of the QCD component is derived from the nonisolated ($I_{\text{rel}} > 0.2$) data. Because of the correlations between $\not{E}_{\text{T}}$ and isolation, the templates for the QCD estimate from the data that are taken from nonisolated samples are modified using the shape taken from the QCD simulation. This treatment is similar in spirit to the QCD treatment in the recent CMS W and Z cross-section measurements [35].

The QCD rate in each jet bin is constrained to the average of the true $\not\!\!E_T$ distribution of the nonisolated region, and the "modified" $\not\!\!E_T$ distribution after accounting for correlations from the Monte Carlo simulation. The QCD component in the fit is constrained to 100 percent of the rate or half the difference between the results, whichever is greater.

The secondary vertex mass shapes for the fit are taken from the nonisolated data. Because of limited statistics, the ≥ 3 jet sample is included as a single template, with separate normalizations for each jet bin.

Similarly, the electron-plus-jets channel is contaminated by photon conversions, jets with a high electromagnetic fraction, and heavy flavor decays. The normalization of this background is also estimated from a fit to the $\not\!\!E_T$ spectrum. However, the nonisolated sidebands do not accurately represent the shape of the $\not\!\!E_T$ distribution, and so the shape is determined by reversing at least two out of six of the electron identification criteria. The ensemble of these "marginal failures" makes a good representation of the shape of the $\not\!\!E_T$ background for this background source. This shape is then fit with the same $\not\!\!E_T$ procedure as in the muon case.

There are alternative control samples for both the jet energy scale, and the b-tag efficiency. The jet energy scale is measured as described in Section 2. The uncertainty measured there is used in a Gaussian constraint on the jet energy scale in the likelihood (approximately 4%). The b-tagging efficiency and light quark mistag rate have been measured in an independent sample of QCD dijet events [36], and these values are input as Gaussian constraints on the parameters in the likelihood. Specifically, the b-tag efficiency scale factor is constrained to 1.0 ± 0.2, and the mistag rate scale factor is constrained to 1.0 ± 0.1. The technical implementation of these efficiencies in the likelihood is to weight the tagged jets in the simulation up or down by the data-to-simulation scale factor, and weight untagged jets in the simulation with zero weight.

The number of predicted events with respect to each contribution is given by Eqns. (1–3), for the $t\bar{t}$ signal and two of the W+jets backgrounds (W+b-jets and W+light flavor). There are similar terms for the other W+jets backgrounds, the single top, and the QCD multijet production. Thus we have

$$\begin{aligned} N^{\text{pred}}_{t\bar{t}}(i,j) &= K_{t\bar{t}} \cdot N^{\text{MC}}_{t\bar{t}}(i,j) \cdot \\ &\quad P^{\text{b tag}}(i,j,R_{\text{b tag}}) \cdot P^{\text{mistag}}(i,j,R_{\text{mistag}}) \cdot P^{\text{JES}}(i,j,R_{\text{JES}}) \end{aligned} \tag{1}$$

$$\begin{aligned} N^{\text{pred}}_{Wb\bar{b}}(i,j) &= K_{Wb\bar{b}} \cdot N^{\text{MC}}_{Wb\bar{b}}(i,j) \cdot \\ &\quad P^{\text{b tag}}(i,j,R_{\text{b tag}}) \cdot P^{\text{mistag}}(i,j,R_{\text{mistag}}) \cdot P^{\text{JES}}(i,j,R_{\text{JES}}) \cdot P^{Q^2}(i,j,R_{Q^2}) \end{aligned} \tag{2}$$

$$\begin{aligned} N^{\text{pred}}_{Wqq}(i,j) &= K_{Wq\bar{q}} \cdot N^{\text{MC}}_{Wqq}(i,j) \cdot \\ &\quad P^{\text{mistag}}(i,j,R_{\text{mistag}}) \cdot P^{\text{JES}}(i,j,R_{\text{JES}}) \cdot P^{Q^2}(i,j,R_{Q^2}) \end{aligned} \tag{3}$$

where $K_{t\bar{t}}$ is the fitted scale factor for the NLO prediction for $t\bar{t}$; i and j run over tags and jets, respectively; $K_{Wb\bar{b}}$ is the fitted scale factor for the NNLO prediction for $Wb\bar{b}$ (etc); $N^{\text{MC}}_x(i,j)$ is the number of events expected for sample X, derived from Monte Carlo and corrected with data-to-Monte-Carlo scale factors. The $P^X(i,j,R_X)$ factors are multiplicative functions accounting for the relative differences with respect to the input expected yield, as a function of the assumed value R_X of nuisance parameter X (i.e., b-tag efficiency, jet energy scale, etc). These are interpolated from various configurations in the simulation with polynomials. The convention chosen is that the nominal event yield is at $R_X = 0$ (i.e., no variation in parameter X), and $P(i,j,R_X) = 1.0$ (i.e., multiplicative factor of 1.0 by default). The "$+1\sigma$" variation is at $R_X = 1$,

and the "-1σ" variation is at $R_X = -1$.

The fit minimizes the negative log likelihood, summing over the histogram bins (k) of the secondary vertex mass, the number of jets (j), and the number of tags (i). The various constraints (described above) are included as Gaussian penalty terms on the variables, which are represented by C_X. The full profile likelihood expression is

$$-2\ln L = -2\left\{ \sum_{i,j}^{\text{tag,jet}} \sum_{k}^{\text{bins}} \left(\ln \mathcal{P}(N_k^{\text{obs}}(i,j), N_k^{\text{exp}}(i,j)) \right) - \frac{1}{2} \sum_{l}^{\text{constraints}} \frac{(C_X - \hat{C}_X)^2}{\sigma^2_{C_X}} \right\} \tag{4}$$

where $\mathcal{P}$ is a Poisson probability that the predicted yield (N^{exp}) given by the various components statistically overlaps with the data (N^{obs}) in each tag/jet bin i, j, given by

$$\ln \mathcal{P}(x, y) = x \ln y - y - \ln \Gamma(x+1) \tag{5}$$

where $\Gamma(x)$ is the Gamma function.

Table 1 shows a summary of all of the inputs to the profile likelihood, as well as the constraints.

Table 1: Inputs to the profile likelihood, along with constraints.

Quantity	Constraint (%)
b-tag Efficiency Scale Factor	20
b-tag Mistag Scale Factor	10
Jet energy scale relative to nominal	4
W+jets renormalization/factorization scales	$^{+100}_{-50}$
W+jets background normalization	unconstrained
QCD background normalization	100
Single-top background normalization	30
Z+jets background normalization	30

There are also a number of systematic uncertainties that are not included directly in the profile likelihood and hence are taken as additional systematic uncertainties outside of the fit result. The largest of these is the systematic uncertainty due to the overall luminosity determination. It has also been shown on independent samples of $Z \to ee$ and $Z \to \mu\mu$ events, that the efficiencies for triggering, reconstructing, and identifying isolated leptons of this type are very similar in the data and simulations. We have corrected for the small differences observed. The effect of these uncertainties are not included in the profile likelihood, and hence are taken as an additional systematic uncertainty of 3%.

There are a number of theoretical uncertainties in the signal modeling that are not included in the profile likelihood at this time. They include differences in the $t\bar{t}$ signal due to renormalization and factorization scales, the amount of initial and final state radiation present, the parton distribution function model, and the matching scale for the matrix-element to parton-shower matching scheme. These are computed from dedicated simulated samples by varying the theoretical parameters of interest according to conservative variations around the reference value. The exception is the parton distribution functions, which are varied by reweighting the sample according to variations in the underlying parton distribution function parameterizations [29]. The numerical impact of each of these is taken as a systematic uncertainty. Specifically these

are 2% for $t\bar{t}$ Q^2 modeling; 2% for initial and final state radiation modeling; 1% for the matrix-element to parton-shower matching in the $t\bar{t}$; and 3% for the parton distribution function differences.

In all of the cases that are described below, the robustness of the statistical procedure is demonstrated with a priori pseudo-experiments where the expected yields and the parameters in the profile likelihood are sampled randomly according to Poisson or Gaussian statistics (as appropriate). In cases where the true frequentist statistical coverage is not achieved due to the limitations of the profile likelihood method, coverage is assured by correcting for the slight biases (of order 1–2% in the central values and/or uncertainties).

4.2 Muon + Jet Analysis

For the muon channel we make two modifications to the basic event selection discussed above. Instead of using the isolation cut of $I_{\mathrm{rel}} < 0.05$, we require that the selected muon tracks are found to be isolated by the particle-flow reconstruction and pass a cut of $I_{\mathrm{rel}} < 0.15$. The results of the fit are shown in Table 2. The fit considers events with one tag (1-tag) and two and more tags (2-tag) separately, giving nine jet-tag 'bins' (subsamples) which are fit by the joint likelihood. Table 2 lists the observed and fitted rates for each jet-tag bin.

Table 2: Results of the fit for muon+jets events with at least 1 b tag.

	Data	Fit	$t\bar{t}$	$t(\bar{t})$	W +b jets	W +c jets	W $+q\bar{q}$	Z +jets	QCD
1 jet 1 b tag	505	504.0	13.3	25.0	94.2	255.1	81.9	13.9	20.6
2 jets 1 b tag	314	318.2	51.0	29.4	82.6	97.7	35.0	7.3	15.1
3 jets 1 b tag	166	158.5	78.3	14.8	29.5	21.9	10.4	2.8	0.8
4 jets 1 b tag	85	89.2	60.6	4.9	12.8	5.5	3.3	1.3	0.8
$\geq$5 jets 1 b tag	45	43.8	34.6	1.5	4.6	1.8	0.9	0.2	0.2
2 jets $\geq$2 b tags	29	24.1	14.7	3.3	5.3	0.5	0.2	0.2	0.0
3 jets $\geq$2 b tags	37	44.0	35.2	3.8	3.9	0.8	0.0	0.2	0.0
4 jets $\geq$2 b tags	41	41.0	36.2	1.9	2.4	0.4	0.0	0.1	0.0
$\geq$5 jets $\geq$2 b tags	27	26.0	24.0	0.8	1.0	0.1	0.1	0.1	0.0
Total	1249	1248.8	347.8	85.4	236.2	383.8	131.8	26.1	37.6

Table 3 lists the systematic uncertainties from the fit. These include both the theoretical uncertainties from the $t\bar{t}$ modeling and the corrections used to match the simulations to the data and give a total uncertainty of 4.3% for the $t\bar{t}$ signal model. The unclustered energy in the detector results in an additional resolution uncertainty of <1% on the $\not{E}_{\mathrm{T}}$ scale. We combine these with the data-simulation uncertainties due to the jet energy scale and jet resolution modeling, the b-tag efficiency and mistag rate and obtain a total systematic uncertainty of 12.5%. For illustrative purposes, in Table 3, we have broken up the pieces of the profile likelihood and quote the uncertainties due to the individual contributions. These are the result of fixing all of the other parameters of the likelihood and only allowing the chosen term to vary.

This yields a cross section measurement of

$$\sigma_{t\bar{t}} = 145 \pm 12\ (\mathrm{stat.}) \pm 18\ (\mathrm{syst.}) \pm 6\ (\mathrm{lumi.})\ \mathrm{pb}, \tag{6}$$

where the last uncertainty corresponds to the 4% uncertainty on the total integrated luminosity [8]. The fit provides in-situ measurements of the scale factors for both b tagging and the jet

Table 3: List of systematic uncertainties for the muon + jet, electron + jet, and combined analyses. Due to the correlation between parameters in the fit, the combined number is not the sum of the squares of the contributions.

Source	Muon Analysis	Electron Analysis	Combined Analysis
Quantity	Uncertainty (%)		
Lepton ID/reco/trigger	3		
$\not{E}_T$ resolution due to unclustered energy	< 1		
$t\bar{t}$+jets Q^2 scale	2		
ISR/FSR	2		
ME to PS matching	2		
PDF	3		
Profile Likelihood Parameter	Uncertainty (%)		
Jet energy scale and resolution	10	9	7
b-tag efficiency	9	8	8
W+jets Q^2 scale	4	3	9
Combined	13	12	12

energy scale. We obtain a result of $98 \pm 6\%$ for the b-tag scale factor and $92 \pm 9\%$ for the jet energy calibration. The scale factors for the W+b jets and W+c jets components indicate that the contributions in the data may be larger than what is expected by the predictions. For the W+b jets component we find a cross section scale factor of $2.6\ ^{+0.8}_{-0.7}$ and for the W+c jets contribution we obtain $1.3\ ^{+0.3}_{-0.2}$. It is also found that the W+jets data are slightly harder than the central value of the renormalization and factorization scales chosen.

4.3 Electron + Jets Analysis

The analysis in the electron channel is performed in the same way as for the muon case. The results are shown in Table 4. The fit was performed in the same manner as for the muon channel, resulting in nine jet-tag 'bins' (subsamples), which were fit by a joint likelihood, as described in Section 4.1. Table 4 lists the observed and fitted rates for each jet-tag bin. Note that the fit parameters are unbounded to avoid problems with bias. This can result in negative values for the event counts, as in the case of the 4 jets 1 tag yield for QCD in Table 4.

Table 4: Results of the electron+jets fit for events with at least 1 b tag.

	Data	Fit	$t\bar{t}$	$t(\bar{t})$	W +b jets	W +c jets	W +$q\bar{q}$	Z +jets	QCD
1 jet 1 b tag	388	389.8	6.0	14.1	42.4	249.5	26.9	3.1	47.9
2 jets 1 b tag	252	245.3	31.7	21.0	44.4	104.0	14.8	3.3	26.2
3 jets 1 b tag	159	156.0	62.7	12.2	23.5	34.4	5.1	2.1	16.0
4 jets 1 b tag	71	80.7	60.6	4.8	8.2	9.2	1.4	0.8	−4.3
$\geq$5 jets 1 b tag	57	52.1	40.9	1.6	2.6	3.0	0.5	0.4	3.0
2 jets $\geq$2 b tags	14	19.9	9.4	2.3	4.7	1.2	0.1	0.2	2.0
3 jets $\geq$2 b tags	39	38.1	29.1	3.1	3.8	0.9	0.0	0.2	0.9
4 jets $\geq$2 b tags	37	41.3	37.1	1.9	1.9	0.4	0.0	0.1	0.0
$\geq$5 jets $\geq$2 b tags	37	30.7	28.8	0.9	0.8	0.2	0.0	0.1	0.0
Total	1054	1053.8	306.3	61.8	132.1	402.7	48.9	10.3	91.6

The resulting cross section is

$$\sigma_{t\bar{t}} = 158 \pm 14\ (\text{stat.}) \pm 19\ (\text{syst.}) \pm 6\ (\text{lumi.})\ \text{pb}. \tag{7}$$

From the fit we obtain a result of $97 \pm 6\%$ for the b-tag scale factor and $103 \pm 8\%$ for the jet energy calibration. The scale factors for the W+b jets and W+c jets components are $1.4\ ^{+0.8}_{-0.6}$ and $1.4\ ^{+0.4}_{-0.3}$, respectively. These are in agreement with the results from the muon channel. The contributions to the systematic uncertainty are summarized in Table 3.

4.4 Simultaneous Muon and Electron Channel Analysis

Having established the consistency of the separate channel measurements, we now proceed to perform a combined fit to both channels. To establish our best measurement, we repeat the fit procedure and apply it simultaneously to the data in both the electron and muon channels. We find that the resulting fitted event yields in each tag category are in good agreement with those obtained from the separate channel fits (Tables 2 and 4). Figure 2 shows the comparison of the corresponding observed and fitted vertex mass distributions. Figure 3 shows the data for ≥ 3 jets and ≥ 1 b-tag, and the fit results for the total transverse energy of the event (H_T), the missing transverse energy (E_T^{miss}), and the transverse mass of the W (M_T^W). We find good agreement in all cases.

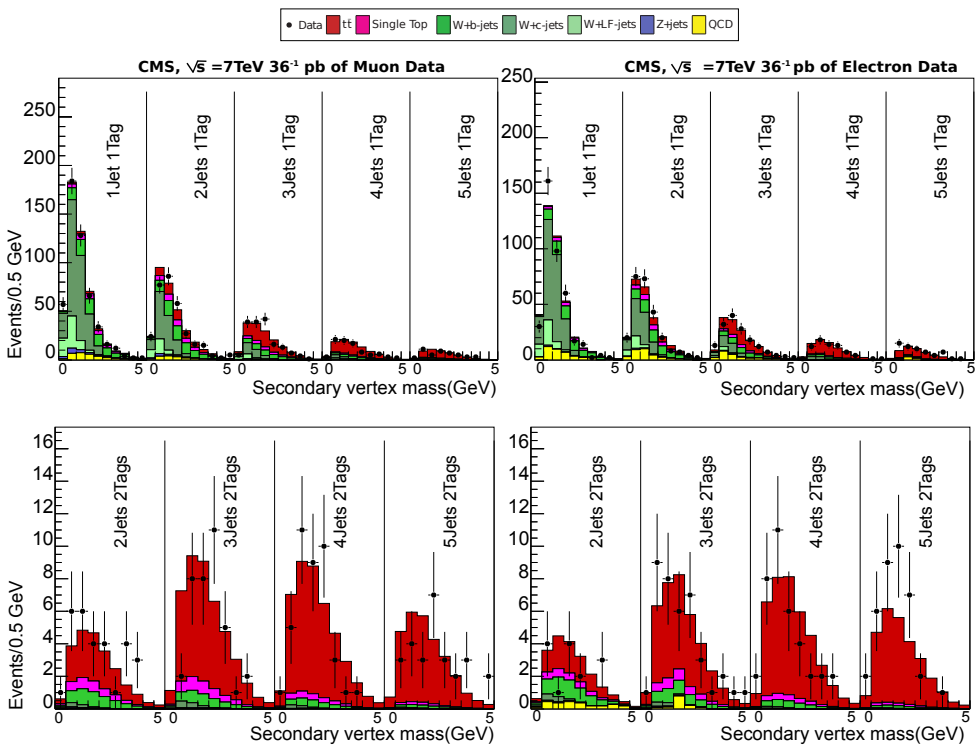

Figure 2: Results of the combined muon and electron channel fit. The muon channel is shown on the left and the electron channel on the right. The plots on the top are for exactly 1 b tag and those on the bottom are for $\geq$2 b tags. The histograms within the top panel correspond to events with 1, 2, 3, 4 and $\geq$5 jets, respectively, while the bottom panel shows histograms corresponding to events with 2, 3, 4 and $\geq$5jets.

The correlation matrix for the combined fit is listed in Table 5. All of the terms are as defined in the text. The combined analysis cross section measurement is

Table 5: Correlation matrix of the fit to the combined electron and muon data samples.

	$t\bar{t}$	$t(\bar{t})$	W +b jets	W +c jets	W $+q\bar{q}$	Z +jets	Q^2	b tag	JES	R_{mistag}
$t\bar{t}$	1.0	−0.1	0.1	0.5	0.2	0.0	0.3	−0.7	−0.6	0.0
$t(\bar{t})$	−0.1	1.0	−0.3	0.0	0.0	0.0	0.1	0.1	0.1	0.0
W+b jets	0.1	−0.3	1.0	0.4	0.4	0.0	0.6	−0.2	0.0	0.0
W+c jets	0.5	0.0	0.4	1.0	−0.1	0.0	0.6	−0.5	−0.2	0.0
W+$q\bar{q}$	0.2	0.0	0.4	−0.1	1.0	−0.1	0.5	−0.2	−0.2	−0.3
Z+jets	0.0	0.0	0.0	0.0	−0.1	1.0	0.0	0.0	0.0	0.0
Q^2	0.3	0.1	0.6	0.6	0.5	0.0	1.0	−0.2	0.1	0.0
b tag	−0.7	−0.1	−0.2	−0.5	−0.2	0.0	−0.2	1.0	0.3	0.0
JES	−0.6	0.1	0.0	−0.2	−0.2	0.0	0.1	0.3	1.0	0.0
R_{mistag}	0.0	0.0	0.0	0.0	−0.3	0.0	0.0	0.0	0.0	1.0

$$\sigma_{t\bar{t}} = 150 \pm 9\ (\text{stat.}) \pm 17\ (\text{syst.}) \pm 6\ (\text{lumi.})\ \text{pb}, \tag{8}$$

which is in good agreement with both the separate channel measurements and those from the cross-check analyses discussed below. The corresponding summary of the systematic uncertainties is given in Table 3. We obtain a result of $96\ ^{+5}_{-4}\%$ for the b-tag scale factor which agrees well with the result obtained in [21]. For the jet energy scale we obtain a result of $107 \pm 6\%$ indicating that the data may prefer a small increase in the jet energy calibration. The scale factors for the W+b jets and W+c jets components indicate that the contributions to the data may be larger than what is predicted by the scaled NNLO predictions of 110 pb and 3.0 nb. For the W+b jets contribution we find a cross section scale factor of $1.9\ ^{+0.6}_{-0.5}$, which is similar to recent observations at the Tevatron [37–39]. The result for the W+c jets contribution is 1.4 ± 0.2.

5 Cross-check Analyses

As a cross-check of our results, we have performed a series of independent analyses in both the muon and electron channels. A summary of these is given in the following subsections. These use not only different analysis techniques but also different methods to suppress the backgrounds from W + jets and QCD multijet events. Each analysis requires at least three jets with $p_T > 25$ GeV and has no requirement on the amount of missing transverse energy. In addition, two different tagging algorithms are used for the two analyses in the muon channel. The Neural Network analysis uses a track counting algorithm which counts the number of tracks nonassociable to the primary vertex [21] and the second analysis uses the muons from semi-leptonic b decays to tag b jets. Each analysis has significantly different systematic uncertainties from the analysis presented above and thus provides a good test of the robustness of the measurements. While there are some differences in the selected event samples, we do not attempt to combine the results because of the substantial overlap.

5.1 Neural Network Analysis with a Track-counting b-tagger

The first cross-check is performed in the muon channel. It makes use of a multi-layer perceptron neural network to distinguish $t\bar{t}$ signal events from the backgrounds after requiring a muon and three jets to pass the selection criteria. The network discriminant is built from the analysis of three input variables: the pseudorapidity $|\eta^\mu|$ of the muon, the distance ΔR_{12} in η–ϕ

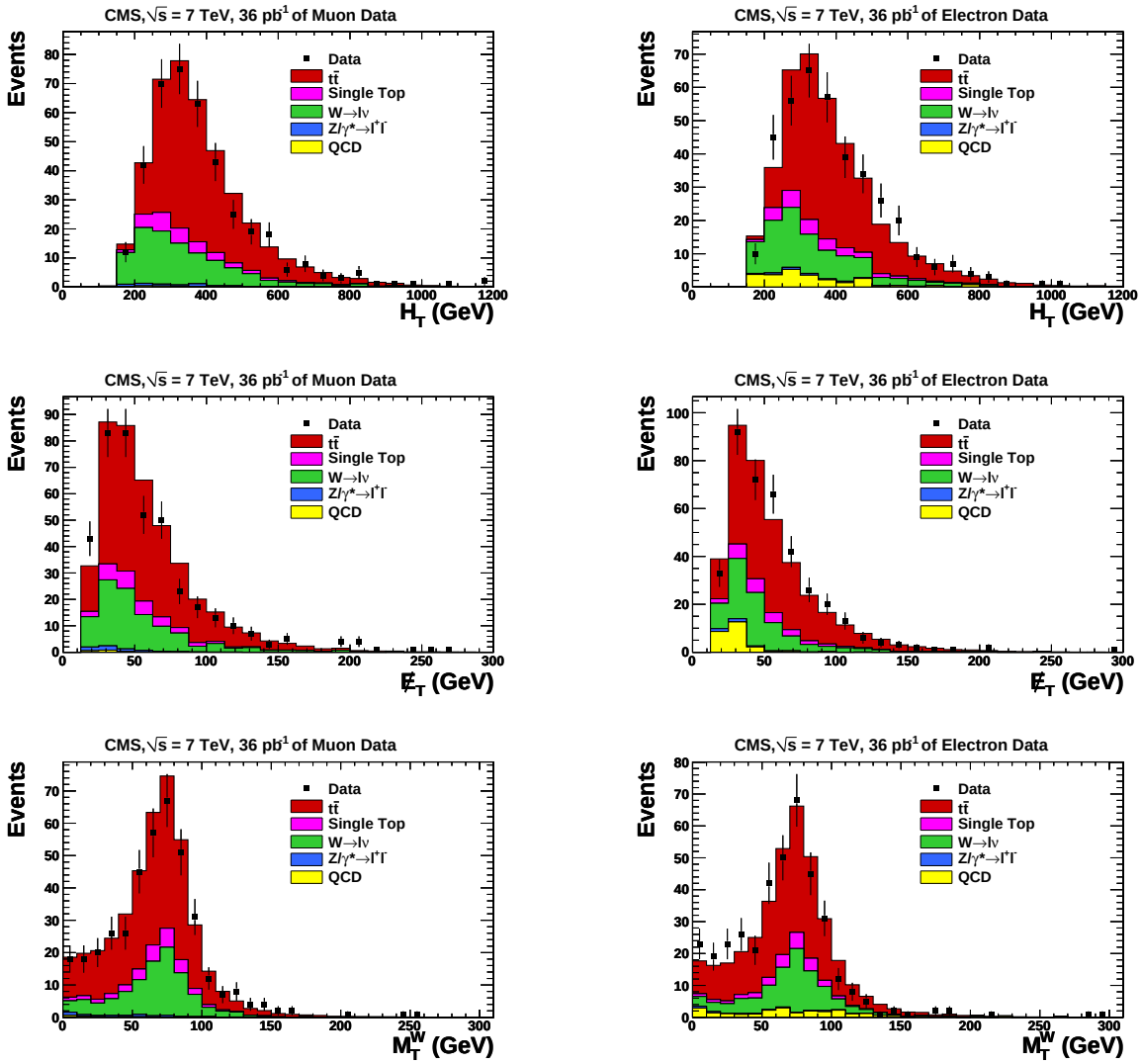

Figure 3: Kinematic distributions of the total transverse energy (H_T), the missing transverse energy (E_T^{miss}) and the transverse mass of the W ($\not{E}_T$). The plots are for $\geq$ 3 jets and $\geq$ 1b tag and the comparison histograms correspond to the fitted values. The muon channel is shown on the left and the electron channel is on the right.

space between the two highest-p_T jets in the event, and a boolean variable indicating the presence of at least one b-tagged jet. The network was trained using simulated samples of signal and background events and the cross section was determined by fitting the sum of signal and background templates to the data.

The signal discriminant was generated from a simulated $t\bar{t}$ sample which was corrected to match the jet energy resolution observed in the data. An additional flavor-dependent correction was applied to the simulated jets to account for differences in b-tag efficiencies between data and simulation. The template shapes for QCD, W+jets, and Z+jets were produced directly from control regions in the data. These were chosen using variables that are only very loosely correlated to the network parameters so that they do not bias the operation of the network.

Because the event topologies of $t\bar{t}$ and single-top events are so similar, there is very little difference in the shapes of the discriminant for the two samples. In order to avoid pathological fit

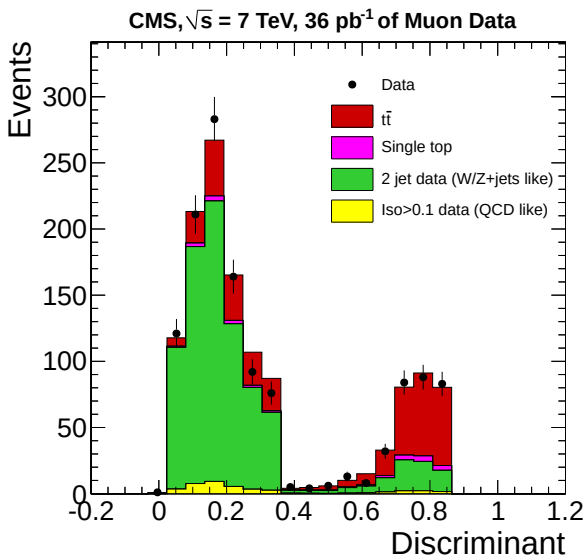

Figure 4: Results of the template fit to the neural network discriminant for 36 pb^{-1} of data.

yields due to this similarity, the number of single-top events in the fit was constrained to the expected yield from the NLO single-top cross section with a 30% uncertainty. The QCD and W/Z+jets likewise share similar shapes in their discriminants. This ambiguity was resolved by constraining the QCD fit yield according to its leading-order (LO) cross section, with a 100% uncertainty due to expected differences between the actual QCD cross section and its LO calculation. However, as the QCD contribution is small, it has little effect on the final result.

The fit of the neural-network discriminant to events passing selection cuts in the data is shown in Fig. 4. A study using pseudo-experiments with simulated data indicates that the fitter introduces a -3.1% bias in the $\mathrm{t\bar{t}}$ yield. This arises due to the use of control regions for the QCD, W+jets, and Z+jets templates. After correcting for this, we obtain a $\mathrm{t\bar{t}}$ event yield of 369 ± 36 (stat.) events.

The systematic uncertainties are evaluated by shifting the simulation by each systematic uncertainty and re-evaluating the result. The resulting pseudo-data are fit with the nominal discriminator templates for $\mathrm{t\bar{t}}$ and single top, and systematically shifted templates for QCD and W/Z+jets. The dominant uncertainty of $^{+16}_{-15}\%$ comes from the b-tag efficiencies. When combined with the other contributions, we find a combined systematic uncertainty of $^{+23}_{-18}\%$. After combining this with the 4% uncertainty in the recorded integrated luminosity [8], we obtain a $\mathrm{t\bar{t}}$ cross section of 151 $\pm$15 (stat.) $^{+35}_{-28}$ (syst.) $\pm$6 (lumi.) pb.

5.2 Muon Channel Analysis using a Muon-in-Jet b-tagger

We have also performed an analysis in which b jets are identified by the presence of a nonisolated muon. The event selection requires at least three well reconstructed jets of which at least one contains a muon with $p_{\mathrm{T}} > 4\,\mathrm{GeV}$ and $|\eta| < 2.4$. The backgrounds from events which come from the decay of a J/ψ, Υ, or Z boson, are excluded using selections on the muon pair invariant mass.

The background from W+b jets and W+c jets with a semimuonic decay and W+light flavor events with a jet that is misidentified as containing a semimuonic decay are estimated from data. We calculate the track taggability from a sample of γ+jet events. This taggability is

convoluted with the track distribution in the jets of the pre-tagged event sample to predict the number of tagged events that should arise from W+jets, $N_{tag,pred}$. We correct for the fraction of events in this sample that are due to QCD multijets, F_{QCD}, to obtain $N_{W+jets} = N_{tag,pred} \cdot (1 - F_{QCD})$. We estimate F_{QCD} using the method discussed below. We assign a 30% systematic uncertainty, based on studies of the taggability parameterization as applied to independent control samples, to the tag-rate prediction to account for the simulation uncertainties.

The QCD background was estimated by calculating the fraction of QCD events in the pre-tag sample. Because of the enrichment in $b\bar{b}$ and $c\bar{c}$ events after requiring the primary muon, a correction factor k is applied to correct for this. The QCD background is then $N_{QCD} = N_{tag,pred} \cdot F_{QCD} \cdot k$. After taking into account the uncertainties in the calculation, we assign a systematic uncertainty in the QCD background of 60%.

The background from Drell–Yan events that survive the Z veto is estimated from simulation. An estimate from data similar to the one described in reference [40] was employed to assign a systematic uncertainty to the prediction from simulation. This gives a systematic uncertainty of 17% on the Z mass veto correction. The remaining backgrounds from diboson and single-top production were estimated from simulated samples that were normalized to the theoretical NLO cross sections. Each of these is assigned a 30% systematic uncertainty.

The selection efficiency for signal events prior to the muon-tag requirement is evaluated using simulated $t\bar{t}$ events and the method described previously. The combined systematic uncertainties on the acceptance, due to the simulation uncertainties, is $^{+6.1}_{-6.9}$%. Because of the relatively soft p_T spectrum of the tag muons, the reconstruction and identification efficiencies were checked using a tag-and-probe analysis [35] of $J/\psi \rightarrow \mu^+\mu^-$ events. The results agree with the simulation to within 1%, so we take the efficiency for finding a tag muon and the mistag efficiency directly from simulation. This gives a tagging efficiency for $t\bar{t}$ events of 25.4 $\pm$ 0.1% excluding the resonance veto requirements, and 23.9 $\pm$ 0.1% including them. The systematic uncertainty on this efficiency is conservatively taken to be 10%. Before calculating the $t\bar{t}$ cross section, the number of predicted tagged events is corrected for the presence of $t\bar{t}$ events in the pre-tag sample. This correction is performed iteratively. Combining these effects gives a total systematic uncertainty on the $t\bar{t}$ cross section due to the background calculations of 17.9%.

Figure 5 shows the observed jet multiplicity distribution, together with the signal and background predictions. Here, the $t\bar{t}$ component is normalized to the NLO cross section [25] and the backgrounds are those computed above. The combined signal and background predictions are in good agreement with the data for each jet multiplicity.

Combining the data yield, the background estimation, the $t\bar{t}$ acceptance, and the tagging efficiency with all of the associated uncertainties, gives a cross section result of 163 $\pm$ 21 (stat.) $\pm$ 35 (syst.) $\pm$ 7 (lumi.) pb. This measurement provides a valuable cross-check of the muon+jets result, as its systematic uncertainties are almost independent of those in the reference analysis.

5.3 Electron Channel Cross-Check Analysis

Our third cross-check analysis is a simple counting analysis using the same displaced vertex tagger as our reference analysis. The event selection requires the presence of at least three well reconstructed jets, of which one or more is required to be b tagged. We estimate the QCD background from the data using control regions in isolation and the W+jets background from a combination of data and simulation. To calculate the $t\bar{t}$ event yield, these are subtracted from the data, along with smaller contributions from single-top, Drell–Yan, and diboson production, which are estimated from simulation.

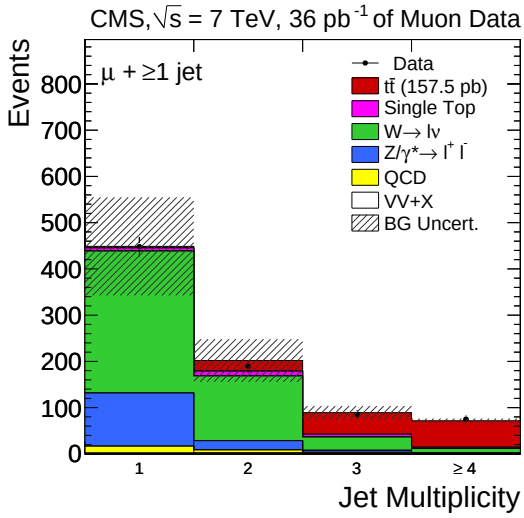

Figure 5: Comparison of data and simulation for the jet multiplicity for events with ≥ 1 muon-in-jet tag. The W+jets and QCD contributions are normalized to the data-driven predictions. The hatched area shows total uncertainty on the background prediction.

The selection efficiency is calculated for $t\bar{t}$ and for W+jets, and the efficiencies to tag individual jets are measured in bins of jet-p_T, separated into b, c, and u, d, s, g (light) partons. The uncertainties from the data are used in systematic studies as well as the statistical uncertainty from the jet efficiency calculations. The resulting predicted b-tag rates applied to simulation of signal and backgrounds are in good agreement with the data (see Fig. 6).

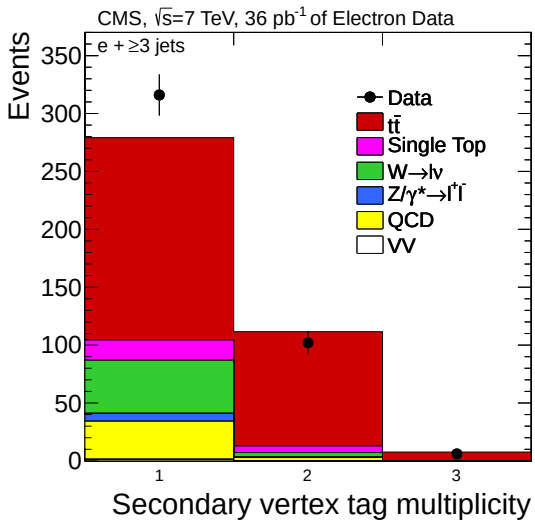

Figure 6: Number of observed and predicted secondary vertex tags in events with ≥ 3 jets.

The QCD background estimation is performed using a fit to the electron I_{rel} distribution in the data above the standard selection where the QCD multijet events dominate. A Gaussian function is used for the central value as it best fits the data, and the fit uncertainty is estimated by varying the I_{rel} range used in the fit and by using alternate fit functions. The systematic uncertainty from $t\bar{t}$ contamination is evaluated by subtracting the number of $t\bar{t}$ events predicted to be inside the fit region using simulation.

The background due to W+jets is estimated using a technique motivated by Berends–Giele

scaling [41] to measure the jet multiplicity distribution before b-tagging. In strict Berends–Giele scaling, the ratio $C(n)$ of events with W+ $\geq n$ jets to events with $W+ \geq (n+1)$ jets is expected to be independent of n. To account for an observed deviation from perfect scaling, in this estimate, $C(n)$ is extracted as a linear function of n, with slope taken from the simulated event sample for $1 \leq n \leq 3$. The W+b jets content in the simulation is scaled up by a factor of two, as determined in Section 4.4.

A W+jets jet multiplicity spectrum in data is prepared by applying an additional requirement on the transverse missing energy, $\not{E}_T > 20$ GeV, to suppress the QCD background. The number of QCD events remaining in these data are then subtracted by refitting the I_{rel} distribution as above. The remaining non-W backgrounds and the $t\bar{t}$ content are subtracted from the data sample using Monte Carlo predictions. The normalization of $C(n)$ is then fitted to this data sample. The scale factors obtained are $C(1) = 4.91 \pm 0.13$ and $C(2) = 5.35 \pm 0.16$, where the uncertainties are statistical. Using $C(n)$ the estimate of the W+jets content in the data with ≥ 3 jets before b tagging ($N^{\text{pretag,data}}$) is

$$N^{\text{pretag,data}}_{\text{W+jets,}\geq\text{3jets}} = \frac{N^{\text{pretag,data}}_{\text{W+jets,}\geq\text{1jets}}}{C(1)C(2)}. \tag{9}$$

The number of tagged W+jet events is then found by applying the selection efficiencies described above.

Systematic uncertainties for the W+jets background estimate are derived by repeating the above process varying $t\bar{t}$ content by 30% as well as varying the normalization of W+b jets by 50% and W+c jets content by factors of 2 and 0.5. Additional fits are also done to Monte Carlo samples where the factorization scale is doubled or halved, as a systematic study. The backgrounds from single-top, Drell-Yan, and diboson production are taken from simulation with a 30% systematic uncertainty.

The background-subtracted and efficiency-corrected yield gives a cross section measurement of $169 \pm 13(\text{stat.})\ ^{+39}_{-32}\ (\text{syst.})\ \pm 7\ (\text{lumi.})$ pb. The dominant systematic uncertainties are the uncertainties on the b-tag scale factors, and the uncertainty on the jet energy scale. This analysis uses a significantly different analysis strategy from the the reference electron+jets analysis but obtains a very similar cross section. Thus it provides a good cross-check of the method and the results.

5.4 Additional Cross-Check

As a further cross-check, the $t\bar{t}$ cross section was also measured in the muon channel using a simple counting analysis which used the same vertex tagger as our reference analysis. The analysis is similar to that of the electron channel analysis described in the previous subsection. The data were selected using a relaxed I_{rel} cut of < 0.1 and a missing transverse energy requirement of $\not{E}_T > 20$ GeV. The QCD multijet background was measured from pre-tagged data using the matrix method [42] and the W + jet background was derived from background-and-signal-subtracted data using the Berends–Giele method described in the Section 5.3. After requiring at least three well reconstructed jets with at least one jet with a b tag and applying a correction of factor of 2 ± 1 for the W + heavy flavor content of the simulated data, we find good agreement between the data and simulations. The resulting cross section is in good agreement with our reference result.

6 Combined CMS Measurement

In addition to the results from this analysis, CMS has also performed a measurement in the dilepton decay channel [43], where we measured a cross section of

$$\text{dileptons: } \sigma_{t\bar{t}} = 168 \pm 18\ (\text{stat.}) \pm 14\ (\text{syst.}) \pm 7\ (\text{lumi.})\ \text{pb}.$$

To produce a final CMS result, we combine this result with the lepton + jets measurement using a profile likelihood method. This procedure uses the vertex mass templates information from this analysis and adds the dilepton measurements as single bin templates. For the dilepton channels, six statistically independent inputs are used so the uncertainty correlations can be handled correctly. These are the eμ events with ≥ 2 jets and no b tag requirement, the eμ, ee, and $\mu\mu$ events with only 1 jet, and the ee and $\mu\mu$ events with ≥ 2 jets and at least 1 b tag. Because different b taggers were used in the two analyses, the b-tag uncertainties are treated as uncorrelated. The 3% PDF uncertainty from the lepton + jets measurement is also treated as uncorrelated because it does not relate to anything in the dilepton analysis. The remaining systematic uncertainties (JES, lepton efficiency, renormalization and factorization scales, ME to PS matching, and ISR/FSR) are all assumed to be correlated. The method was verified by using pseudo-experiments, from which it was determined that the likelihood calculation resulted in a 10% underestimate of the errors. We correct for the underestimate in the final result and obtain a combined measurement of

$$\text{CMS combined: } \sigma_{t\bar{t}} = 154 \pm 17\ (\text{stat.} + \text{syst.}) \pm 6\ (\text{lumi.})\ \text{pb}.$$

Figure 7 shows the comparison of the separate and combined CMS [10, 43] measurements of the production cross section. The inner error bars on the data points correspond to the statistical uncertainty, while the outer (thinner) error bars correspond to the quadratic sum of the statistical and systematic uncertainties. The outermost brackets correspond to the total uncertainty, including a luminosity uncertainty of 11% (4%) for the 3 (36) pb^{-1} results, respectively, which is also added in quadrature.

Also shown are NLO and approximate NNLO QCD calculations, for comparison. These were computed using the HATHOR program [5] using the calculations from [6]. A common factorization and renormalization scale of $Q = m_t = 173\,\text{GeV}$ was used for the calculations together with the MRTSW 2008 NNLO (NLO) parton distribution functions. The scale uncertainty was determined by independently varying the two scales by factors of 2 and 0.5 and taking the maximum variation as the uncertainty. The PDF uncertainty corresponds to the 90% confidence level (C.L.) uncertainties for the parton distribution functions [29]. This is added in quadrature to the scale uncertainty.

In Fig. 8 we compare these and the $p\bar{p}$ results from the Tevatron [37, 38, 44, 45] to the theoretical predictions as a function of $\sqrt{s}$. These are from the approximate NNLO QCD calculations referred to above and the width of the error band corresponds to the variation resulting from changing the Q^2 scale up and down by a factor of 2. We find good agreement between the data and the theory in all cases and we note that the combined measurement is already more precise than the NLO QCD prediction.

7 Summary of Results

We have presented the results of a new analysis of the $t\bar{t}$ production cross section at $\sqrt{s} = 7\,\text{TeV}$ using data recorded by the CMS detector at the LHC during 2010 corresponding to an inte-

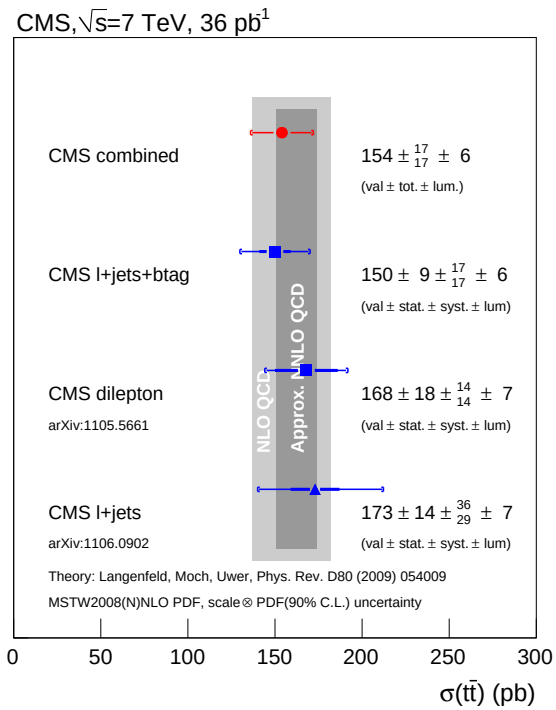

Figure 7: Comparison of the CMS measurements for the $t\bar{t}$ production cross sections and the QCD predictions for $\sqrt{s} = 7\,\text{TeV}$

grated luminosity of $36\,\text{pb}^{-1}$. Using muon and electron+jets and using b tagging to suppress the backgrounds, we measure cross sections of

$$\mu\text{+jets: } \sigma_{t\bar{t}} = 145 \pm 12\ (\text{stat.}) \pm 18\ (\text{syst.}) \pm 6\ (\text{lumi.})\ \text{pb},$$
$$\text{e+jets: } \sigma_{t\bar{t}} = 158 \pm 14\ (\text{stat.}) \pm 19\ (\text{syst.}) \pm 6\ (\text{lumi.})\ \text{pb},$$

from the separate channels. The combination of these gives a cross section of

$$l\text{+jets: } \sigma_{t\bar{t}} = 150 \pm 9\ (\text{stat.}) \pm 17\ (\text{syst.}) \pm 6\ (\text{lumi.})\ \text{pb}.$$

When combined with the CMS dilepton measurement, we obtain an improved cross section measurement of

$$\text{CMS combined: } \sigma_{t\bar{t}} = 154 \pm 17\ (\text{stat.} + \text{syst.}) \pm 6\ (\text{lumi.})\ \text{pb}.$$

The measurements are in good agreement with the QCD predictions of 164^{+10}_{-13} pb [5, 6] and 163^{+11}_{-10} pb [7] which are based on the full NLO matrix elements and the resummation of the leading and next-to-leading soft logarithms.

Acknowledgements

We wish to congratulate our colleagues in the CERN accelerator departments for the excellent performance of the LHC machine. We thank the technical and administrative staff at

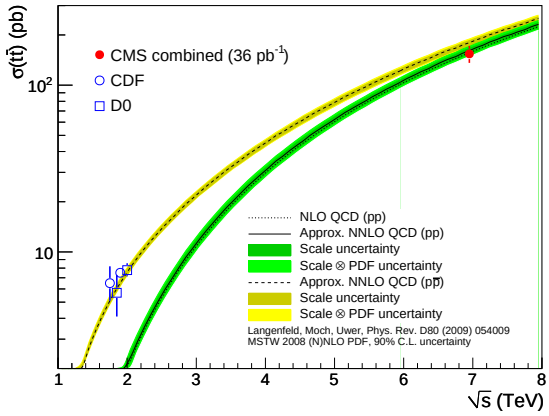

Figure 8: Comparison of the CMS and Tevatron results for the $t\bar{t}$ production cross section with QCD as a function of $\sqrt{s}$

CERN and other CMS Institutes, and acknowledge support from: FMSR (Austria); FNRS and FWO (Belgium); CNPq, CAPES, FAPERJ, and FAPESP (Brazil); MES (Bulgaria); CERN; CAS, MoST, and NSFC (China); COLCIENCIAS (Colombia); MSES (Croatia); RPF (Cyprus); Academy of Sciences and NICPB (Estonia); Academy of Finland, ME, and HIP (Finland); CEA and CNRS/IN2P3 (France); BMBF, DFG, and HGF (Germany); GSRT (Greece); OTKA and NKTH (Hungary); DAE and DST (India); IPM (Iran); SFI (Ireland); INFN (Italy); NRF (Korea); LAS (Lithuania); CINVESTAV, CONACYT, SEP, and UASLP-FAI (Mexico); PAEC (Pakistan); SCSR (Poland); FCT (Portugal); JINR (Armenia, Belarus, Georgia, Ukraine, Uzbekistan); MST and MAE (Russia); MSTDS (Serbia); MICINN and CPAN (Spain); Swiss Funding Agencies (Switzerland); NSC (Taipei); TUBITAK and TAEK (Turkey); STFC (United Kingdom); DOE and NSF (USA). Individuals have received support from the Marie-Curie IEF program (European Union); the Leventis Foundation; the A. P. Sloan Foundation; the Alexander von Humboldt Foundation; and the World Class University program by NRF (Korea).

References

[1] CDF Collaboration, "Observation of top quark production in $\bar{p}p$ collisions", *Phys. Rev. Lett.* **74** (1995) 2626, arXiv:9503002. doi:10.1103/PhysRevLett.74.2626.

[2] D0 Collaboration, "Observation of the top quark", *Phys. Rev. Lett.* **74** (1995) 2632, arXiv:9503003. doi:10.1103/PhysRevLett.74.2632.

[3] J. R. Incandela et al., "Status and Prospects of Top-Quark Physics", *Prog. Part. Nucl. Phys.* **63** (2009) 239, arXiv:0904.2499. doi:10.1016/j.ppnp.2009.08.001.

[4] L. Evans and P. Bryant (editors), "LHC Machine", *JINST* **03** (2008) S08001. doi:10.1088/1748-0221/3/08/S08001.

[5] M. Aliev et al., "HATHOR: HAdronic Top and Heavy quarks crOss section calculatoR", *Comput. Phys. Commun.* **182** (2011) 1034, arXiv:1007.1327. doi:10.1016/j.cpc.2010.12.040.

[6] U. Langenfeld, S. Moch, and P. Uwer, "Measuring the running top-quark mass", *Phys. Rev. D* **80** (2009) 054009, arXiv:0906.5273. doi:10.1103/PhysRevD.80.054009.

[7] N. Kidonakis, "Next-to-next-to-leading soft-gluon corrections for the top quark cross section and transverse momentum distribution", *Phys. Rev. D* **82** (2010) 114030, arXiv:1009.4935. doi:10.1103/PhysRevD.82.114030.

[8] CMS Collaboration, "Measurement of CMS Luminosity", CMS Physics Analysis Summary CMS-PAS-EWK-10-004, (2010).

[9] CMS Collaboration, "First Measurement of the Cross Section for Top-Quark Pair Production in Proton-Proton Collisions at 7 TeV", *Phys. Lett. B* **695** (2011) 424. doi:10.1016/j.physletb.2010.11.058.

[10] CMS Collaboration, "Measurement of the $t\bar{t}$ Pair Production Cross Section using the Kinematic Properties of Lepton + Jets Events", (2011). arXiv:1106.0902. Submitted to *Eur. Phys. J. C*.

[11] ATLAS Collaboration, "Measurement of the top quark-pair production cross section with ATLAS in pp collisions at $\sqrt{s}$ = 7 TeV", (2010). arXiv:1012.1792. Accepted by *Eur. Phys. J. C*.

[12] CMS Collaboration, "The CMS experiment at the CERN LHC", *JINST* **3** (2008) S08004. doi:10.1088/1748-0221/3/08/S08004.

[13] CMS Collaboration, "Performance of muon identification in pp collisions at $\sqrt{s}$ = 7 TeV", CMS Physics Analysis Summary CMS-PAS-MUO-10-002, (2010).

[14] CMS Collaboration, "Electron Reconstruction and Identification at $\sqrt{s} = 7$ TeV", CMS Physics Analysis Summary CMS-PAS-EGM-10-004, (2010).

[15] CMS Collaboration, "CMS Tracking Performance Results from Early LHC Operation", *Eur. Phys. J. C* **70** (2010) 1165. doi:10.1140/epjc/s10052-010-1491-3.

[16] CMS Collaboration, "Commissioning of the Particle-Flow Reconstruction in Minimum-Bias and Jet Events from pp Collisions at 7 TeV", CMS Physics Analysis Summary CMS-PAS-PFT-10-002, (2010).

[17] M. Cacciari, G. P. Salam, and G. Soyez, "The anti-kt jet clustering algorithm", *JHEP* **04** (2008) 063. doi:10.1088/1126-6708/2008/04/063.

[18] M. Cacciari and G. P. Salam, "Dispelling the N**3 myth for the k(t) jet-finder", *Phys. Lett. B* **641** (2006) 57, arXiv:hep-ph/0512210. doi:10.1016/j.physletb.2006.08.037.

[19] M. Cacciari, G. P. Salam, and G. Soyez, "Fastjet Package", (2011).

[20] CMS Collaboration, "Determination of the Jet Energy Scale in CMS with pp Collisions at $\sqrt{s} = 7$ TeV", CMS Physics Analysis Summary CMS-PAS-JME-10-010, (2010).

[21] CMS Collaboration, "Algorithms for b Jet Identification in CMS", CMS Physics Analysis Summary CMS-PAS-BTV-09-001, (2009).

[22] J. Alwall et al., "MadGraph/MadEvent v4: The New Web Generation", *JHEP* **09** (2007) 028. doi:10.1088/1126-6708/2007/09/028.

[23] T. Sjöstrand, S. Mrenna, and P. Z. Skands, "PYTHIA 6.4 Physics and Manual", *JHEP* **05** (2006) 026, arXiv:0603175. doi:10.1088/1126-6708/2006/05/026.

[24] J. Allison et al., "Geant4 developments and applications", *IEEE Trans. Nucl. Sci.* **53** (2006) 270. doi:10.1109/TNS.2006.869826.

[25] J. Campbell and R. Ellis, "MCFM for the Tevatron and the LHC", (2010). arXiv:1007.3492.

[26] A. D. Martin, W. J. Stirling, R. S. Thorne et al., "Uncertainties on α_s in global PDF analyses and implications for predicted hadronic cross sections", *Eur. Phys. J. C* **64** (2009) 653, arXiv:0905.3531. doi:10.1140/epjc/s10052-009-1164-2.

[27] H.-L. Lai et al., "Uncertainty induced by QCD coupling in the CTEQ-TEA global analysis of parton distributions", *Phys. Rev. D* **82** (2010) 054021, arXiv:1004.4624. doi:10.1103/PhysRevD.82.054021.

[28] F. Demartin, S. Forte, E. Mariani et al., "The impact of PDF and α_s uncertainties on Higgs Production in gluon fusion at hadron colliders", *Phys. Rev. D* **82** (2010) 014002, arXiv:1004.0962. doi:10.1103/PhysRevD.82.014002.

[29] PDF4LHC Working Group, "PDF4LHC Recommendations", (2010).

[30] J. M. Campbell, R. Frederix, F. Maltoni et al., "Next-to-Leading-Order Predictions for t-Channel Single-Top Production at Hadron Colliders", *Phys. Rev. Lett.* **102** (2009) 182003, arXiv:0903.0005. doi:10.1103/PhysRevLett.102.182003.

[31] J. M. Campbell and F. Tramontano, "Next-to-leading order corrections to W t production and decay", *Nucl. Phys. B* **726** (2005) 109, arXiv:0506289. doi:10.1016/j.nuclphysb.2005.08.015.

[32] J. M. Campbell, R. K. Ellis, and F. Tramontano, "Single top production and decay at next-to-leading order", *Phys. Rev. D* **70** (2004) 094012, arXiv:hep-ph/0408158. doi:10.1103/PhysRevD.70.094012.

[33] CMS Collaboration, "Measurement of the single-top t-channel cross section in pp collisions at $\sqrt{s} = 7$ TeV", CMS Physics Analysis Summary CMS-PAS-TOP-10-008, (2010).

[34] K. Melnikov and F. Petriello, "Electroweak gauge boson production at hadron colliders through $O(\alpha_s^2)$", *Phys. Rev. D* **74** (2006) 114017, arXiv:hep-ph/0609070. doi:10.1103/PhysRevD.74.114017.

[35] CMS Collaboration, "Measurements of Inclusive W and Z Cross Sections in pp Collisions at $\sqrt{s}$ = 7 TeV", *JHEP* **01** (2011) 080. doi:10.1007/JHEP01(2011)080.

[36] CMS Collaboration, "Commissioning of b-jet identification with pp collisions at $\sqrt{s}$ = 7 TeV", CMS Physics Analysis Summary CMS-PAS-BTV-10-001, (2010).

[37] D0 Collaboration, "Measurement of the top quark pair production cross section in the lepton+jets channel in proton-antiproton collisions at $\sqrt{s}$ = 1.96 TeV", *Phys. Rev. D* **84** (2011) 012008, arXiv:1101.0124. doi:10.1103/PhysRevD.84.012008.

[38] CDF Collaboration, "Combination of CDF top quark pair production measurements with up to 4.6 fb^{-1}", CDF Note 9913, (2009).

[39] CDF Collaboration, "First measurement of the b-jet cross section in events with a W boson in proton-antiproton collisions at $\sqrt{s}$ = 1.96 TeV", *Phys. Rev. Lett.* **104** (2010) 131801, arXiv:0909.1505. doi:10.1103/PhysRevLett.104.131801.

[40] CDF Collaboration, "Measurement of the $t\bar{t}$ production cross-section in $p\bar{p}$ collisions at $\sqrt{s} = 1.96$ TeV using lepton plus jets events with semileptonic B decays to muons", *Phys. Rev. D* **72** (2005) 032002, arXiv:0506001. doi:10.1103/PhysRevD.72.032002.

[41] F. A. Berends et al., "On the production of a W and jets at hadron colliders", *Nucl. Phys. B* **357** (1991) 32. doi:10.1016/0550-3213(91)90458-A.

[42] D0 Collaboration, "Measurement of the t anti-t production cross section in p anti-p collisions at $\sqrt{s} = 1.96$ TeV using secondary vertex b tagging", *Phys. Rev. D* **74** (2006) 112004, arXiv:0611002. doi:10.1103/PhysRevD.74.112004.

[43] CMS Collaboration, "Measurement of the top-quark pair production cross section and the top-quark mass in the dilepton channel at $\sqrt{s}$ = 7 TeV", *JHEP* **7** (2011) 49. doi:10.1007/JHEP07(2011)049.

[44] D0 Collaboration, "t anti-t production cross-section in p anti-p collisions at $\sqrt{s} = 1.8$ TeV", *Phys. Rev. D* **67** (2003) 012004, arXiv:0205019. doi:10.1103/PhysRevD.67.012004.

[45] CDF Collaboration, "Measurement of the t anti-t production cross-section in p anti-p collisions at $\sqrt{s} = 1.8$ TeV", *Phys. Rev. D* **64** (2001) 032002, arXiv:0101036. doi:10.1103/PhysRevD.64.032002.

CDF Collaboration, "Erratum: Measurement of the t anti-t production cross-section in p anti-p collisions at $\sqrt{s} = 1.8$ TeV", *Phys. Rev. D* **67** (2003) 119901(E). doi:10.1103/PhysRevD.67.119901.

A The CMS Collaboration

Yerevan Physics Institute, Yerevan, Armenia
S. Chatrchyan, V. Khachatryan, A.M. Sirunyan, A. Tumasyan

Institut für Hochenergiephysik der OeAW, Wien, Austria
W. Adam, T. Bergauer, M. Dragicevic, J. Erö, C. Fabjan, M. Friedl, R. Frühwirth, V.M. Ghete, J. Hammer[1], S. Hänsel, M. Hoch, N. Hörmann, J. Hrubec, M. Jeitler, W. Kiesenhofer, M. Krammer, D. Liko, I. Mikulec, M. Pernicka, B. Rahbaran, H. Rohringer, R. Schöfbeck, J. Strauss, A. Taurok, F. Teischinger, P. Wagner, W. Waltenberger, G. Walzel, E. Widl, C.-E. Wulz

National Centre for Particle and High Energy Physics, Minsk, Belarus
V. Mossolov, N. Shumeiko, J. Suarez Gonzalez

Universiteit Antwerpen, Antwerpen, Belgium
S. Bansal, L. Benucci, E.A. De Wolf, X. Janssen, J. Maes, T. Maes, L. Mucibello, S. Ochesanu, B. Roland, R. Rougny, M. Selvaggi, H. Van Haevermaet, P. Van Mechelen, N. Van Remortel

Vrije Universiteit Brussel, Brussel, Belgium
F. Blekman, S. Blyweert, J. D'Hondt, O. Devroede, R. Gonzalez Suarez, A. Kalogeropoulos, M. Maes, W. Van Doninck, P. Van Mulders, G.P. Van Onsem, I. Villella

Université Libre de Bruxelles, Bruxelles, Belgium
O. Charaf, B. Clerbaux, G. De Lentdecker, V. Dero, A.P.R. Gay, G.H. Hammad, T. Hreus, P.E. Marage, L. Thomas, C. Vander Velde, P. Vanlaer

Ghent University, Ghent, Belgium
V. Adler, A. Cimmino, S. Costantini, M. Grunewald, B. Klein, J. Lellouch, A. Marinov, J. Mccartin, D. Ryckbosch, F. Thyssen, M. Tytgat, L. Vanelderen, P. Verwilligen, S. Walsh, N. Zaganidis

Université Catholique de Louvain, Louvain-la-Neuve, Belgium
S. Basegmez, G. Bruno, J. Caudron, L. Ceard, E. Cortina Gil, J. De Favereau De Jeneret, C. Delaere, D. Favart, A. Giammanco, G. Grégoire, J. Hollar, V. Lemaitre, J. Liao, O. Militaru, C. Nuttens, S. Ovyn, D. Pagano, A. Pin, K. Piotrzkowski, N. Schul

Université de Mons, Mons, Belgium
N. Beliy, T. Caebergs, E. Daubie

Centro Brasileiro de Pesquisas Fisicas, Rio de Janeiro, Brazil
G.A. Alves, L. Brito, D. De Jesus Damiao, M.E. Pol, M.H.G. Souza

Universidade do Estado do Rio de Janeiro, Rio de Janeiro, Brazil
W.L. Aldá Júnior, W. Carvalho, E.M. Da Costa, C. De Oliveira Martins, S. Fonseca De Souza, D. Matos Figueiredo, L. Mundim, H. Nogima, V. Oguri, W.L. Prado Da Silva, A. Santoro, S.M. Silva Do Amaral, A. Sznajder

Instituto de Fisica Teorica, Universidade Estadual Paulista, Sao Paulo, Brazil
C.A. Bernardes[2], F.A. Dias, T.R. Fernandez Perez Tomei, E. M. Gregores[2], C. Lagana, F. Marinho, P.G. Mercadante[2], S.F. Novaes, Sandra S. Padula

Institute for Nuclear Research and Nuclear Energy, Sofia, Bulgaria
N. Darmenov[1], V. Genchev[1], P. Iaydjiev[1], S. Piperov, M. Rodozov, S. Stoykova, G. Sultanov, V. Tcholakov, R. Trayanov

University of Sofia, Sofia, Bulgaria
A. Dimitrov, R. Hadjiiska, A. Karadzhinova, V. Kozhuharov, L. Litov, M. Mateev, B. Pavlov, P. Petkov

Institute of High Energy Physics, Beijing, China
J.G. Bian, G.M. Chen, H.S. Chen, C.H. Jiang, D. Liang, S. Liang, X. Meng, J. Tao, J. Wang, J. Wang, X. Wang, Z. Wang, H. Xiao, M. Xu, J. Zang, Z. Zhang

State Key Lab. of Nucl. Phys. and Tech., Peking University, Beijing, China
Y. Ban, S. Guo, Y. Guo, W. Li, Y. Mao, S.J. Qian, H. Teng, B. Zhu, W. Zou

Universidad de Los Andes, Bogota, Colombia
A. Cabrera, B. Gomez Moreno, A.A. Ocampo Rios, A.F. Osorio Oliveros, J.C. Sanabria

Technical University of Split, Split, Croatia
N. Godinovic, D. Lelas, K. Lelas, R. Plestina[3], D. Polic, I. Puljak

University of Split, Split, Croatia
Z. Antunovic, M. Dzelalija

Institute Rudjer Boskovic, Zagreb, Croatia
V. Brigljevic, S. Duric, K. Kadija, S. Morovic

University of Cyprus, Nicosia, Cyprus
A. Attikis, M. Galanti, J. Mousa, C. Nicolaou, F. Ptochos, P.A. Razis

Charles University, Prague, Czech Republic
M. Finger, M. Finger Jr.

Academy of Scientific Research and Technology of the Arab Republic of Egypt, Egyptian Network of High Energy Physics, Cairo, Egypt
Y. Assran[4], A. Ellithi Kamel, S. Khalil[5], M.A. Mahmoud[6]

National Institute of Chemical Physics and Biophysics, Tallinn, Estonia
A. Hektor, M. Kadastik, M. Müntel, M. Raidal, L. Rebane, A. Tiko

Department of Physics, University of Helsinki, Helsinki, Finland
V. Azzolini, P. Eerola, G. Fedi

Helsinki Institute of Physics, Helsinki, Finland
S. Czellar, J. Härkönen, A. Heikkinen, V. Karimäki, R. Kinnunen, M.J. Kortelainen, T. Lampén, K. Lassila-Perini, S. Lehti, T. Lindén, P. Luukka, T. Mäenpää, E. Tuominen, J. Tuominiemi, E. Tuovinen, D. Ungaro, L. Wendland

Lappeenranta University of Technology, Lappeenranta, Finland
K. Banzuzi, A. Karjalainen, A. Korpela, T. Tuuva

Laboratoire d'Annecy-le-Vieux de Physique des Particules, IN2P3-CNRS, Annecy-le-Vieux, France
D. Sillou

DSM/IRFU, CEA/Saclay, Gif-sur-Yvette, France
M. Besancon, S. Choudhury, M. Dejardin, D. Denegri, B. Fabbro, J.L. Faure, F. Ferri, S. Ganjour, F.X. Gentit, A. Givernaud, P. Gras, G. Hamel de Monchenault, P. Jarry, E. Locci, J. Malcles, M. Marionneau, L. Millischer, J. Rander, A. Rosowsky, I. Shreyber, M. Titov, P. Verrecchia

Laboratoire Leprince-Ringuet, Ecole Polytechnique, IN2P3-CNRS, Palaiseau, France
S. Baffioni, F. Beaudette, L. Benhabib, L. Bianchini, M. Bluj[7], C. Broutin, P. Busson, C. Charlot, T. Dahms, L. Dobrzynski, S. Elgammal, R. Granier de Cassagnac, M. Haguenauer, P. Miné, C. Mironov, C. Ochando, P. Paganini, D. Sabes, R. Salerno, Y. Sirois, C. Thiebaux, B. Wyslouch[8], A. Zabi

Institut Pluridisciplinaire Hubert Curien, Université de Strasbourg, Université de Haute Alsace Mulhouse, CNRS/IN2P3, Strasbourg, France
J.-L. Agram[9], J. Andrea, D. Bloch, D. Bodin, J.-M. Brom, M. Cardaci, E.C. Chabert, C. Collard, E. Conte[9], F. Drouhin[9], C. Ferro, J.-C. Fontaine[9], D. Gelé, U. Goerlach, S. Greder, P. Juillot, M. Karim[9], A.-C. Le Bihan, Y. Mikami, P. Van Hove

Centre de Calcul de l'Institut National de Physique Nucleaire et de Physique des Particules (IN2P3), Villeurbanne, France
F. Fassi, D. Mercier

Université de Lyon, Université Claude Bernard Lyon 1, CNRS-IN2P3, Institut de Physique Nucléaire de Lyon, Villeurbanne, France
C. Baty, S. Beauceron, N. Beaupere, M. Bedjidian, O. Bondu, G. Boudoul, D. Boumediene, H. Brun, J. Chasserat, R. Chierici, D. Contardo, P. Depasse, H. El Mamouni, J. Fay, S. Gascon, B. Ille, T. Kurca, T. Le Grand, M. Lethuillier, L. Mirabito, S. Perries, V. Sordini, S. Tosi, Y. Tschudi, P. Verdier

Institute of High Energy Physics and Informatization, Tbilisi State University, Tbilisi, Georgia
D. Lomidze

RWTH Aachen University, I. Physikalisches Institut, Aachen, Germany
G. Anagnostou, S. Beranek, M. Edelhoff, L. Feld, N. Heracleous, O. Hindrichs, R. Jussen, K. Klein, J. Merz, N. Mohr, A. Ostapchuk, A. Perieanu, F. Raupach, J. Sammet, S. Schael, D. Sprenger, H. Weber, M. Weber, B. Wittmer

RWTH Aachen University, III. Physikalisches Institut A, Aachen, Germany
M. Ata, E. Dietz-Laursonn, M. Erdmann, T. Hebbeker, C. Heidemann, A. Hinzmann, K. Hoepfner, T. Klimkovich, D. Klingebiel, P. Kreuzer, D. Lanske[†], J. Lingemann, C. Magass, M. Merschmeyer, A. Meyer, P. Papacz, H. Pieta, H. Reithler, S.A. Schmitz, L. Sonnenschein, J. Steggemann, D. Teyssier

RWTH Aachen University, III. Physikalisches Institut B, Aachen, Germany
M. Bontenackels, M. Davids, M. Duda, G. Flügge, H. Geenen, M. Giffels, W. Haj Ahmad, D. Heydhausen, F. Hoehle, B. Kargoll, T. Kress, Y. Kuessel, A. Linn, A. Nowack, L. Perchalla, O. Pooth, J. Rennefeld, P. Sauerland, A. Stahl, M. Thomas, D. Tornier, M.H. Zoeller

Deutsches Elektronen-Synchrotron, Hamburg, Germany
M. Aldaya Martin, W. Behrenhoff, U. Behrens, M. Bergholz[10], A. Bethani, K. Borras, A. Cakir, A. Campbell, E. Castro, D. Dammann, G. Eckerlin, D. Eckstein, A. Flossdorf, G. Flucke, A. Geiser, J. Hauk, H. Jung[1], M. Kasemann, I. Katkov[11], P. Katsas, C. Kleinwort, H. Kluge, A. Knutsson, M. Krämer, D. Krücker, E. Kuznetsova, W. Lange, W. Lohmann[10], R. Mankel, M. Marienfeld, I.-A. Melzer-Pellmann, A.B. Meyer, J. Mnich, A. Mussgiller, J. Olzem, A. Petrukhin, D. Pitzl, A. Raspereza, A. Raval, M. Rosin, R. Schmidt[10], T. Schoerner-Sadenius, N. Sen, A. Spiridonov, M. Stein, J. Tomaszewska, R. Walsh, C. Wissing

University of Hamburg, Hamburg, Germany
C. Autermann, V. Blobel, S. Bobrovskyi, J. Draeger, H. Enderle, U. Gebbert, M. Görner,

T. Hermanns, K. Kaschube, G. Kaussen, H. Kirschenmann, R. Klanner, J. Lange, B. Mura, S. Naumann-Emme, F. Nowak, N. Pietsch, C. Sander, H. Schettler, P. Schleper, E. Schlieckau, M. Schröder, T. Schum, H. Stadie, G. Steinbrück, J. Thomsen

Institut für Experimentelle Kernphysik, Karlsruhe, Germany
C. Barth, J. Bauer, J. Berger, V. Buege, T. Chwalek, W. De Boer, A. Dierlamm, G. Dirkes, M. Feindt, J. Gruschke, C. Hackstein, F. Hartmann, M. Heinrich, H. Held, K.H. Hoffmann, S. Honc, J.R. Komaragiri, T. Kuhr, D. Martschei, S. Mueller, Th. Müller, M. Niegel, O. Oberst, A. Oehler, J. Ott, T. Peiffer, G. Quast, K. Rabbertz, F. Ratnikov, N. Ratnikova, M. Renz, C. Saout, A. Scheurer, P. Schieferdecker, F.-P. Schilling, G. Schott, H.J. Simonis, F.M. Stober, D. Troendle, J. Wagner-Kuhr, T. Weiler, M. Zeise, V. Zhukov[11], E.B. Ziebarth

Institute of Nuclear Physics "Demokritos", Aghia Paraskevi, Greece
G. Daskalakis, T. Geralis, S. Kesisoglou, A. Kyriakis, D. Loukas, I. Manolakos, A. Markou, C. Markou, C. Mavrommatis, E. Ntomari, E. Petrakou

University of Athens, Athens, Greece
L. Gouskos, T.J. Mertzimekis, A. Panagiotou, E. Stiliaris

University of Ioánnina, Ioánnina, Greece
I. Evangelou, C. Foudas, P. Kokkas, N. Manthos, I. Papadopoulos, V. Patras, F.A. Triantis

KFKI Research Institute for Particle and Nuclear Physics, Budapest, Hungary
A. Aranyi, G. Bencze, L. Boldizsar, C. Hajdu[1], P. Hidas, D. Horvath[12], A. Kapusi, K. Krajczar[13], F. Sikler[1], G.I. Veres[13], G. Vesztergombi[13]

Institute of Nuclear Research ATOMKI, Debrecen, Hungary
N. Beni, J. Molnar, J. Palinkas, Z. Szillasi, V. Veszpremi

University of Debrecen, Debrecen, Hungary
P. Raics, Z.L. Trocsanyi, B. Ujvari

Panjab University, Chandigarh, India
S.B. Beri, V. Bhatnagar, N. Dhingra, R. Gupta, M. Jindal, M. Kaur, J.M. Kohli, M.Z. Mehta, N. Nishu, L.K. Saini, A. Sharma, A.P. Singh, J. Singh, S.P. Singh

University of Delhi, Delhi, India
S. Ahuja, B.C. Choudhary, P. Gupta, S. Jain, A. Kumar, A. Kumar, M. Naimuddin, K. Ranjan, R.K. Shivpuri

Saha Institute of Nuclear Physics, Kolkata, India
S. Banerjee, S. Bhattacharya, S. Dutta, B. Gomber, S. Jain, R. Khurana, S. Sarkar

Bhabha Atomic Research Centre, Mumbai, India
R.K. Choudhury, D. Dutta, S. Kailas, V. Kumar, P. Mehta, A.K. Mohanty[1], L.M. Pant, P. Shukla

Tata Institute of Fundamental Research - EHEP, Mumbai, India
T. Aziz, M. Guchait[14], A. Gurtu, M. Maity[15], D. Majumder, G. Majumder, K. Mazumdar, G.B. Mohanty, A. Saha, K. Sudhakar, N. Wickramage

Tata Institute of Fundamental Research - HECR, Mumbai, India
S. Banerjee, S. Dugad, N.K. Mondal

Institute for Research and Fundamental Sciences (IPM), Tehran, Iran
H. Arfaei, H. Bakhshiansohi[16], S.M. Etesami, A. Fahim[16], M. Hashemi, H. Hesari, A. Jafari[16],

M. Khakzad, A. Mohammadi[17], M. Mohammadi Najafabadi, S. Paktinat Mehdiabadi, B. Safarzadeh, M. Zeinali[18]

INFN Sezione di Bari [a], Università di Bari [b], Politecnico di Bari [c], Bari, Italy
M. Abbrescia[a,b], L. Barbone[a,b], C. Calabria[a,b], A. Colaleo[a], D. Creanza[a,c], N. De Filippis[a,c,1], M. De Palma[a,b], L. Fiore[a], G. Iaselli[a,c], L. Lusito[a,b], G. Maggi[a,c], M. Maggi[a], N. Manna[a,b], B. Marangelli[a,b], S. My[a,c], S. Nuzzo[a,b], N. Pacifico[a,b], G.A. Pierro[a], A. Pompili[a,b], G. Pugliese[a,c], F. Romano[a,c], G. Roselli[a,b], G. Selvaggi[a,b], L. Silvestris[a], R. Trentadue[a], S. Tupputi[a,b], G. Zito[a]

INFN Sezione di Bologna [a], Università di Bologna [b], Bologna, Italy
G. Abbiendi[a], A.C. Benvenuti[a], D. Bonacorsi[a], S. Braibant-Giacomelli[a,b], L. Brigliadori[a], P. Capiluppi[a,b], A. Castro[a,b], F.R. Cavallo[a], M. Cuffiani[a,b], G.M. Dallavalle[a], F. Fabbri[a], A. Fanfani[a,b], D. Fasanella[a], P. Giacomelli[a], M. Giunta[a], C. Grandi[a], S. Marcellini[a], G. Masetti[b], M. Meneghelli[a,b], A. Montanari[a], F.L. Navarria[a,b], F. Odorici[a], A. Perrotta[a], F. Primavera[a], A.M. Rossi[a,b], T. Rovelli[a,b], G. Siroli[a,b], R. Travaglini[a,b]

INFN Sezione di Catania [a], Università di Catania [b], Catania, Italy
S. Albergo[a,b], G. Cappello[a,b], M. Chiorboli[a,b,1], S. Costa[a,b], A. Tricomi[a,b], C. Tuve[a,b]

INFN Sezione di Firenze [a], Università di Firenze [b], Firenze, Italy
G. Barbagli[a], V. Ciulli[a,b], C. Civinini[a], R. D'Alessandro[a,b], E. Focardi[a,b], S. Frosali[a,b], E. Gallo[a], S. Gonzi[a,b], P. Lenzi[a,b], M. Meschini[a], S. Paoletti[a], G. Sguazzoni[a], A. Tropiano[a,1]

INFN Laboratori Nazionali di Frascati, Frascati, Italy
L. Benussi, S. Bianco, S. Colafranceschi[19], F. Fabbri, D. Piccolo

INFN Sezione di Genova, Genova, Italy
P. Fabbricatore, R. Musenich

INFN Sezione di Milano-Bicocca [a], Università di Milano-Bicocca [b], Milano, Italy
A. Benaglia[a,b], F. De Guio[a,b,1], L. Di Matteo[a,b], S. Gennai[1], A. Ghezzi[a,b], S. Malvezzi[a], A. Martelli[a,b], A. Massironi[a,b], D. Menasce[a], L. Moroni[a], M. Paganoni[a,b], D. Pedrini[a], S. Ragazzi[a,b], N. Redaelli[a], S. Sala[a], T. Tabarelli de Fatis[a,b]

INFN Sezione di Napoli [a], Università di Napoli "Federico II" [b], Napoli, Italy
S. Buontempo[a], C.A. Carrillo Montoya[a,1], N. Cavallo[a,20], A. De Cosa[a,b], F. Fabozzi[a,20], A.O.M. Iorio[a,1], L. Lista[a], M. Merola[a,b], P. Paolucci[a]

INFN Sezione di Padova [a], Università di Padova [b], Università di Trento (Trento) [c], Padova, Italy
P. Azzi[a], N. Bacchetta[a], P. Bellan[a,b], D. Bisello[a,b], A. Branca[a], R. Carlin[a,b], P. Checchia[a], T. Dorigo[a], U. Dosselli[a], F. Fanzago[a], F. Gasparini[a,b], U. Gasparini[a,b], A. Gozzelino, S. Lacaprara[a,21], I. Lazzizzera[a,c], M. Margoni[a,b], M. Mazzucato[a], A.T. Meneguzzo[a,b], M. Nespolo[a,1], L. Perrozzi[a,1], N. Pozzobon[a,b], P. Ronchese[a,b], F. Simonetto[a,b], E. Torassa[a], M. Tosi[a,b], S. Vanini[a,b], P. Zotto[a,b], G. Zumerle[a,b]

INFN Sezione di Pavia [a], Università di Pavia [b], Pavia, Italy
P. Baesso[a,b], U. Berzano[a], S.P. Ratti[a,b], C. Riccardi[a,b], P. Torre[a,b], P. Vitulo[a,b], C. Viviani[a,b]

INFN Sezione di Perugia [a], Università di Perugia [b], Perugia, Italy
M. Biasini[a,b], G.M. Bilei[a], B. Caponeri[a,b], L. Fanò[a,b], P. Lariccia[a,b], A. Lucaroni[a,b,1], G. Mantovani[a,b], M. Menichelli[a], A. Nappi[a,b], F. Romeo[a,b], A. Santocchia[a,b], S. Taroni[a,b,1], M. Valdata[a,b]

INFN Sezione di Pisa [a], Università di Pisa [b], Scuola Normale Superiore di Pisa [c], Pisa, Italy
P. Azzurri[a,c], G. Bagliesi[a], J. Bernardini[a,b], T. Boccali[a,1], G. Broccolo[a,c], R. Castaldi[a], R.T. D'Agnolo[a,c], R. Dell'Orso[a], F. Fiori[a,b], L. Foà[a,c], A. Giassi[a], A. Kraan[a], F. Ligabue[a,c], T. Lomtadze[a], L. Martini[a,22], A. Messineo[a,b], F. Palla[a], G. Segneri[a], A.T. Serban[a], P. Spagnolo[a], R. Tenchini[a], G. Tonelli[a,b,1], A. Venturi[a,1], P.G. Verdini[a]

INFN Sezione di Roma [a], Università di Roma "La Sapienza" [b], Roma, Italy
L. Barone[a,b], F. Cavallari[a], D. Del Re[a,b], E. Di Marco[a,b], M. Diemoz[a], D. Franci[a,b], M. Grassi[a,1], E. Longo[a,b], P. Meridiani, S. Nourbakhsh[a], G. Organtini[a,b], F. Pandolfi[a,b,1], R. Paramatti[a], S. Rahatlou[a,b], C. Rovelli[1]

INFN Sezione di Torino [a], Università di Torino [b], Università del Piemonte Orientale (Novara) [c], Torino, Italy
N. Amapane[a,b], R. Arcidiacono[a,c], S. Argiro[a,b], M. Arneodo[a,c], C. Biino[a], C. Botta[a,b,1], N. Cartiglia[a], R. Castello[a,b], M. Costa[a,b], N. Demaria[a], A. Graziano[a,b,1], C. Mariotti[a], M. Marone[a,b], S. Maselli[a], E. Migliore[a,b], G. Mila[a,b], V. Monaco[a,b], M. Musich[a,b], M.M. Obertino[a,c], N. Pastrone[a], M. Pelliccioni[a,b], A. Potenza[a,b], A. Romero[a,b], M. Ruspa[a,c], R. Sacchi[a,b], V. Sola[a,b], A. Solano[a,b], A. Staiano[a], A. Vilela Pereira[a]

INFN Sezione di Trieste [a], Università di Trieste [b], Trieste, Italy
S. Belforte[a], F. Cossutti[a], G. Della Ricca[a,b], B. Gobbo[a], D. Montanino[a,b], A. Penzo[a]

Kangwon National University, Chunchon, Korea
S.G. Heo, S.K. Nam

Kyungpook National University, Daegu, Korea
S. Chang, J. Chung, D.H. Kim, G.N. Kim, J.E. Kim, D.J. Kong, H. Park, S.R. Ro, D.C. Son, T. Son

Chonnam National University, Institute for Universe and Elementary Particles, Kwangju, Korea
J.Y. Kim, Zero J. Kim, S. Song

Korea University, Seoul, Korea
S. Choi, B. Hong, M. Jo, H. Kim, J.H. Kim, T.J. Kim, K.S. Lee, D.H. Moon, S.K. Park, K.S. Sim

University of Seoul, Seoul, Korea
M. Choi, S. Kang, H. Kim, C. Park, I.C. Park, S. Park, G. Ryu

Sungkyunkwan University, Suwon, Korea
Y. Choi, Y.K. Choi, J. Goh, M.S. Kim, J. Lee, S. Lee, H. Seo, I. Yu

Vilnius University, Vilnius, Lithuania
M.J. Bilinskas, I. Grigelionis, M. Janulis, D. Martisiute, P. Petrov, T. Sabonis

Centro de Investigacion y de Estudios Avanzados del IPN, Mexico City, Mexico
H. Castilla-Valdez, E. De La Cruz-Burelo, I. Heredia-de La Cruz, R. Lopez-Fernandez, R. Magaña Villalba, A. Sánchez-Hernández, L.M. Villasenor-Cendejas

Universidad Iberoamericana, Mexico City, Mexico
S. Carrillo Moreno, F. Vazquez Valencia

Benemerita Universidad Autonoma de Puebla, Puebla, Mexico
H.A. Salazar Ibarguen

Universidad Autónoma de San Luis Potosí, San Luis Potosí, Mexico
E. Casimiro Linares, A. Morelos Pineda, M.A. Reyes-Santos

University of Auckland, Auckland, New Zealand
D. Krofcheck, J. Tam

University of Canterbury, Christchurch, New Zealand
P.H. Butler, R. Doesburg, H. Silverwood

National Centre for Physics, Quaid-I-Azam University, Islamabad, Pakistan
M. Ahmad, I. Ahmed, M.I. Asghar, H.R. Hoorani, W.A. Khan, T. Khurshid, S. Qazi

Institute of Experimental Physics, Faculty of Physics, University of Warsaw, Warsaw, Poland
G. Brona, M. Cwiok, W. Dominik, K. Doroba, A. Kalinowski, M. Konecki, J. Krolikowski

Soltan Institute for Nuclear Studies, Warsaw, Poland
T. Frueboes, R. Gokieli, M. Górski, M. Kazana, K. Nawrocki, K. Romanowska-Rybinska, M. Szleper, G. Wrochna, P. Zalewski

Laboratório de Instrumentação e Física Experimental de Partículas, Lisboa, Portugal
N. Almeida, P. Bargassa, A. David, P. Faccioli, P.G. Ferreira Parracho, M. Gallinaro[1], P. Musella, A. Nayak, J. Pela[1], P.Q. Ribeiro, J. Seixas, J. Varela

Joint Institute for Nuclear Research, Dubna, Russia
S. Afanasiev, I. Belotelov, P. Bunin, I. Golutvin, A. Kamenev, V. Karjavin, G. Kozlov, A. Lanev, P. Moisenz, V. Palichik, V. Perelygin, S. Shmatov, V. Smirnov, A. Volodko, A. Zarubin

Petersburg Nuclear Physics Institute, Gatchina (St Petersburg), Russia
V. Golovtsov, Y. Ivanov, V. Kim, P. Levchenko, V. Murzin, V. Oreshkin, I. Smirnov, V. Sulimov, L. Uvarov, S. Vavilov, A. Vorobyev, An. Vorobyev

Institute for Nuclear Research, Moscow, Russia
Yu. Andreev, A. Dermenev, S. Gninenko, N. Golubev, M. Kirsanov, N. Krasnikov, V. Matveev, A. Pashenkov, A. Toropin, S. Troitsky

Institute for Theoretical and Experimental Physics, Moscow, Russia
V. Epshteyn, V. Gavrilov, V. Kaftanov[†], M. Kossov[1], A. Krokhotin, N. Lychkovskaya, V. Popov, G. Safronov, S. Semenov, V. Stolin, E. Vlasov, A. Zhokin

Moscow State University, Moscow, Russia
E. Boos, M. Dubinin[23], L. Dudko, A. Ershov, A. Gribushin, O. Kodolova, I. Lokhtin, A. Markina, S. Obraztsov, M. Perfilov, S. Petrushanko, L. Sarycheva, V. Savrin, A. Snigirev

P.N. Lebedev Physical Institute, Moscow, Russia
V. Andreev, M. Azarkin, I. Dremin, M. Kirakosyan, A. Leonidov, S.V. Rusakov, A. Vinogradov

State Research Center of Russian Federation, Institute for High Energy Physics, Protvino, Russia
I. Azhgirey, I. Bayshev, S. Bitioukov, V. Grishin[1], V. Kachanov, D. Konstantinov, A. Korablev, V. Krychkine, V. Petrov, R. Ryutin, A. Sobol, L. Tourtchanovitch, S. Troshin, N. Tyurin, A. Uzunian, A. Volkov

University of Belgrade, Faculty of Physics and Vinca Institute of Nuclear Sciences, Belgrade, Serbia
P. Adzic[24], M. Djordjevic, D. Krpic[24], J. Milosevic

Centro de Investigaciones Energéticas Medioambientales y Tecnológicas (CIEMAT), Madrid, Spain
M. Aguilar-Benitez, J. Alcaraz Maestre, P. Arce, C. Battilana, E. Calvo, M. Cepeda, M. Cerrada,

M. Chamizo Llatas, N. Colino, B. De La Cruz, A. Delgado Peris, C. Diez Pardos, D. Domínguez Vázquez, C. Fernandez Bedoya, J.P. Fernández Ramos, A. Ferrando, J. Flix, M.C. Fouz, P. Garcia-Abia, O. Gonzalez Lopez, S. Goy Lopez, J.M. Hernandez, M.I. Josa, G. Merino, J. Puerta Pelayo, I. Redondo, L. Romero, J. Santaolalla, M.S. Soares, C. Willmott

Universidad Autónoma de Madrid, Madrid, Spain
C. Albajar, G. Codispoti, J.F. de Trocóniz

Universidad de Oviedo, Oviedo, Spain
J. Cuevas, J. Fernandez Menendez, S. Folgueras, I. Gonzalez Caballero, L. Lloret Iglesias, J.M. Vizan Garcia

Instituto de Física de Cantabria (IFCA), CSIC-Universidad de Cantabria, Santander, Spain
J.A. Brochero Cifuentes, I.J. Cabrillo, A. Calderon, S.H. Chuang, J. Duarte Campderros, M. Felcini[25], M. Fernandez, G. Gomez, J. Gonzalez Sanchez, C. Jorda, P. Lobelle Pardo, A. Lopez Virto, J. Marco, R. Marco, C. Martinez Rivero, F. Matorras, F.J. Munoz Sanchez, J. Piedra Gomez[26], T. Rodrigo, A.Y. Rodríguez-Marrero, A. Ruiz-Jimeno, L. Scodellaro, M. Sobron Sanudo, I. Vila, R. Vilar Cortabitarte

CERN, European Organization for Nuclear Research, Geneva, Switzerland
D. Abbaneo, E. Auffray, G. Auzinger, P. Baillon, A.H. Ball, D. Barney, A.J. Bell[27], D. Benedetti, C. Bernet[3], W. Bialas, P. Bloch, A. Bocci, S. Bolognesi, M. Bona, H. Breuker, K. Bunkowski, T. Camporesi, G. Cerminara, T. Christiansen, J.A. Coarasa Perez, B. Curé, D. D'Enterria, A. De Roeck, S. Di Guida, N. Dupont-Sagorin, A. Elliott-Peisert, B. Frisch, W. Funk, A. Gaddi, G. Georgiou, H. Gerwig, D. Gigi, K. Gill, D. Giordano, F. Glege, R. Gomez-Reino Garrido, M. Gouzevitch, P. Govoni, S. Gowdy, L. Guiducci, M. Hansen, C. Hartl, J. Harvey, J. Hegeman, B. Hegner, H.F. Hoffmann, A. Honma, V. Innocente, P. Janot, K. Kaadze, E. Karavakis, P. Lecoq, C. Lourenço, T. Mäki, M. Malberti, L. Malgeri, M. Mannelli, L. Masetti, A. Maurisset, F. Meijers, S. Mersi, E. Meschi, R. Moser, M.U. Mozer, M. Mulders, E. Nesvold[1], M. Nguyen, T. Orimoto, L. Orsini, E. Palencia Cortezon, E. Perez, A. Petrilli, A. Pfeiffer, M. Pierini, M. Pimiä, D. Piparo, G. Polese, A. Racz, W. Reece, J. Rodrigues Antunes, G. Rolandi[28], T. Rommerskirchen, M. Rovere, H. Sakulin, C. Schäfer, C. Schwick, I. Segoni, A. Sharma, P. Siegrist, P. Silva, M. Simon, P. Sphicas[29], M. Spiropulu[23], M. Stoye, P. Tropea, A. Tsirou, P. Vichoudis, M. Voutilainen, W.D. Zeuner

Paul Scherrer Institut, Villigen, Switzerland
W. Bertl, K. Deiters, W. Erdmann, K. Gabathuler, R. Horisberger, Q. Ingram, H.C. Kaestli, S. König, D. Kotlinski, U. Langenegger, F. Meier, D. Renker, T. Rohe, J. Sibille[30], A. Starodumov[31]

Institute for Particle Physics, ETH Zurich, Zurich, Switzerland
L. Bäni, P. Bortignon, L. Caminada[32], B. Casal, N. Chanon, Z. Chen, S. Cittolin, G. Dissertori, M. Dittmar, J. Eugster, K. Freudenreich, C. Grab, W. Hintz, P. Lecomte, W. Lustermann, C. Marchica[32], P. Martinez Ruiz del Arbol, P. Milenovic[33], F. Moortgat, C. Nägeli[32], P. Nef, F. Nessi-Tedaldi, L. Pape, F. Pauss, T. Punz, A. Rizzi, F.J. Ronga, M. Rossini, L. Sala, A.K. Sanchez, M.-C. Sawley, B. Stieger, L. Tauscher[†], A. Thea, K. Theofilatos, D. Treille, C. Urscheler, R. Wallny, M. Weber, L. Wehrli, J. Weng

Universität Zürich, Zurich, Switzerland
E. Aguilo, C. Amsler, V. Chiochia, S. De Visscher, C. Favaro, M. Ivova Rikova, B. Millan Mejias, P. Otiougova, P. Robmann, A. Schmidt, H. Snoek

National Central University, Chung-Li, Taiwan
Y.H. Chang, K.H. Chen, C.M. Kuo, S.W. Li, W. Lin, Z.K. Liu, Y.J. Lu, D. Mekterovic, R. Volpe, J.H. Wu, S.S. Yu

National Taiwan University (NTU), Taipei, Taiwan
P. Bartalini, P. Chang, Y.H. Chang, Y.W. Chang, Y. Chao, K.F. Chen, W.-S. Hou, Y. Hsiung, K.Y. Kao, Y.J. Lei, R.-S. Lu, J.G. Shiu, Y.M. Tzeng, M. Wang

Cukurova University, Adana, Turkey
A. Adiguzel, M.N. Bakirci[34], S. Cerci[35], C. Dozen, I. Dumanoglu, E. Eskut, S. Girgis, G. Gokbulut, I. Hos, E.E. Kangal, A. Kayis Topaksu, G. Onengut, K. Ozdemir, S. Ozturk[36], A. Polatoz, K. Sogut[37], D. Sunar Cerci[35], B. Tali[35], H. Topakli[34], D. Uzun, L.N. Vergili, M. Vergili

Middle East Technical University, Physics Department, Ankara, Turkey
I.V. Akin, T. Aliev, B. Bilin, S. Bilmis, M. Deniz, H. Gamsizkan, A.M. Guler, K. Ocalan, A. Ozpineci, M. Serin, R. Sever, U.E. Surat, E. Yildirim, M. Zeyrek

Bogazici University, Istanbul, Turkey
M. Deliomeroglu, D. Demir[38], E. Gülmez, B. Isildak, M. Kaya[39], O. Kaya[39], M. Özbek, S. Ozkorucuklu[40], N. Sonmez[41]

National Scientific Center, Kharkov Institute of Physics and Technology, Kharkov, Ukraine
L. Levchuk

University of Bristol, Bristol, United Kingdom
F. Bostock, J.J. Brooke, T.L. Cheng, E. Clement, D. Cussans, R. Frazier, J. Goldstein, M. Grimes, D. Hartley, G.P. Heath, H.F. Heath, L. Kreczko, S. Metson, D.M. Newbold[42], K. Nirunpong, A. Poll, S. Senkin, V.J. Smith

Rutherford Appleton Laboratory, Didcot, United Kingdom
L. Basso[43], K.W. Bell, A. Belyaev[43], C. Brew, R.M. Brown, B. Camanzi, D.J.A. Cockerill, J.A. Coughlan, K. Harder, S. Harper, J. Jackson, B.W. Kennedy, E. Olaiya, D. Petyt, B.C. Radburn-Smith, C.H. Shepherd-Themistocleous, I.R. Tomalin, W.J. Womersley, S.D. Worm

Imperial College, London, United Kingdom
R. Bainbridge, G. Ball, J. Ballin, R. Beuselinck, O. Buchmuller, D. Colling, N. Cripps, M. Cutajar, G. Davies, M. Della Negra, W. Ferguson, J. Fulcher, D. Futyan, A. Gilbert, A. Guneratne Bryer, G. Hall, Z. Hatherell, J. Hays, G. Iles, M. Jarvis, G. Karapostoli, L. Lyons, B.C. MacEvoy, A.-M. Magnan, J. Marrouche, B. Mathias, R. Nandi, J. Nash, A. Nikitenko[31], A. Papageorgiou, M. Pesaresi, K. Petridis, M. Pioppi[44], D.M. Raymond, S. Rogerson, N. Rompotis, A. Rose, M.J. Ryan, C. Seez, P. Sharp, A. Sparrow, A. Tapper, S. Tourneur, M. Vazquez Acosta, T. Virdee, S. Wakefield, N. Wardle, D. Wardrope, T. Whyntie

Brunel University, Uxbridge, United Kingdom
M. Barrett, M. Chadwick, J.E. Cole, P.R. Hobson, A. Khan, P. Kyberd, D. Leslie, W. Martin, I.D. Reid, L. Teodorescu

Baylor University, Waco, USA
K. Hatakeyama, H. Liu

The University of Alabama, Tuscaloosa, USA
C. Henderson

Boston University, Boston, USA
T. Bose, E. Carrera Jarrin, C. Fantasia, A. Heister, J. St. John, P. Lawson, D. Lazic, J. Rohlf, D. Sperka, L. Sulak

Brown University, Providence, USA
A. Avetisyan, S. Bhattacharya, J.P. Chou, D. Cutts, A. Ferapontov, U. Heintz, S. Jabeen, G. Kukartsev, G. Landsberg, M. Luk, M. Narain, D. Nguyen, M. Segala, T. Sinthuprasith, T. Speer, K.V. Tsang

University of California, Davis, Davis, USA
R. Breedon, G. Breto, M. Calderon De La Barca Sanchez, S. Chauhan, M. Chertok, J. Conway, P.T. Cox, J. Dolen, R. Erbacher, E. Friis, W. Ko, A. Kopecky, R. Lander, H. Liu, S. Maruyama, T. Miceli, M. Nikolic, D. Pellett, J. Robles, S. Salur, T. Schwarz, M. Searle, J. Smith, M. Squires, M. Tripathi, R. Vasquez Sierra, C. Veelken

University of California, Los Angeles, Los Angeles, USA
V. Andreev, K. Arisaka, D. Cline, R. Cousins, A. Deisher, J. Duris, S. Erhan, C. Farrell, J. Hauser, M. Ignatenko, C. Jarvis, C. Plager, G. Rakness, P. Schlein[†], J. Tucker, V. Valuev

University of California, Riverside, Riverside, USA
J. Babb, A. Chandra, R. Clare, J. Ellison, J.W. Gary, F. Giordano, G. Hanson, G.Y. Jeng, S.C. Kao, F. Liu, H. Liu, O.R. Long, A. Luthra, H. Nguyen, B.C. Shen[†], R. Stringer, J. Sturdy, S. Sumowidagdo, R. Wilken, S. Wimpenny

University of California, San Diego, La Jolla, USA
W. Andrews, J.G. Branson, G.B. Cerati, D. Evans, F. Golf, A. Holzner, R. Kelley, M. Lebourgeois, J. Letts, B. Mangano, S. Padhi, C. Palmer, G. Petrucciani, H. Pi, M. Pieri, R. Ranieri, M. Sani, V. Sharma, S. Simon, E. Sudano, M. Tadel, Y. Tu, A. Vartak, S. Wasserbaech[45], F. Würthwein, A. Yagil, J. Yoo

University of California, Santa Barbara, Santa Barbara, USA
D. Barge, R. Bellan, C. Campagnari, M. D'Alfonso, T. Danielson, K. Flowers, P. Geffert, J. Incandela, C. Justus, P. Kalavase, S.A. Koay, D. Kovalskyi, V. Krutelyov, S. Lowette, N. Mccoll, V. Pavlunin, F. Rebassoo, J. Ribnik, J. Richman, R. Rossin, D. Stuart, W. To, J.R. Vlimant

California Institute of Technology, Pasadena, USA
A. Apresyan, A. Bornheim, J. Bunn, Y. Chen, M. Gataullin, Y. Ma, A. Mott, H.B. Newman, C. Rogan, K. Shin, V. Timciuc, P. Traczyk, J. Veverka, R. Wilkinson, Y. Yang, R.Y. Zhu

Carnegie Mellon University, Pittsburgh, USA
B. Akgun, R. Carroll, T. Ferguson, Y. Iiyama, D.W. Jang, S.Y. Jun, Y.F. Liu, M. Paulini, J. Russ, H. Vogel, I. Vorobiev

University of Colorado at Boulder, Boulder, USA
J.P. Cumalat, M.E. Dinardo, B.R. Drell, C.J. Edelmaier, W.T. Ford, A. Gaz, B. Heyburn, E. Luiggi Lopez, U. Nauenberg, J.G. Smith, K. Stenson, K.A. Ulmer, S.R. Wagner, S.L. Zang

Cornell University, Ithaca, USA
L. Agostino, J. Alexander, D. Cassel, A. Chatterjee, N. Eggert, L.K. Gibbons, B. Heltsley, K. Henriksson, W. Hopkins, A. Khukhunaishvili, B. Kreis, G. Nicolas Kaufman, J.R. Patterson, D. Puigh, A. Ryd, M. Saelim, E. Salvati, X. Shi, W. Sun, W.D. Teo, J. Thom, J. Thompson, J. Vaughan, Y. Weng, L. Winstrom, P. Wittich

Fairfield University, Fairfield, USA
A. Biselli, G. Cirino, D. Winn

Fermi National Accelerator Laboratory, Batavia, USA
S. Abdullin, M. Albrow, J. Anderson, G. Apollinari, M. Atac, J.A. Bakken, L.A.T. Bauerdick, A. Beretvas, J. Berryhill, P.C. Bhat, I. Bloch, F. Borcherding, K. Burkett, J.N. Butler, V. Chetluru, H.W.K. Cheung, F. Chlebana, S. Cihangir, W. Cooper, D.P. Eartly, V.D. Elvira, S. Esen, I. Fisk, J. Freeman, Y. Gao, E. Gottschalk, D. Green, K. Gunthoti, O. Gutsche, J. Hanlon, R.M. Harris, J. Hirschauer, B. Hooberman, H. Jensen, M. Johnson, U. Joshi, R. Khatiwada, B. Klima, K. Kousouris, S. Kunori, S. Kwan, C. Leonidopoulos, P. Limon, D. Lincoln, R. Lipton, J. Lykken, K. Maeshima, J.M. Marraffino, D. Mason, P. McBride, T. Miao, K. Mishra, S. Mrenna, Y. Musienko[46], C. Newman-Holmes, V. O'Dell, R. Pordes, O. Prokofyev, N. Saoulidou, E. Sexton-Kennedy, S. Sharma, W.J. Spalding, L. Spiegel, P. Tan, L. Taylor, S. Tkaczyk, L. Uplegger, E.W. Vaandering, R. Vidal, J. Whitmore, W. Wu, F. Yang, F. Yumiceva, J.C. Yun

University of Florida, Gainesville, USA
D. Acosta, P. Avery, D. Bourilkov, M. Chen, S. Das, M. De Gruttola, G.P. Di Giovanni, D. Dobur, A. Drozdetskiy, R.D. Field, M. Fisher, Y. Fu, I.K. Furic, J. Gartner, J. Hugon, B. Kim, J. Konigsberg, A. Korytov, A. Kropivnitskaya, T. Kypreos, J.F. Low, K. Matchev, G. Mitselmakher, L. Muniz, C. Prescott, R. Remington, A. Rinkevicius, M. Schmitt, B. Scurlock, P. Sellers, N. Skhirtladze, M. Snowball, D. Wang, J. Yelton, M. Zakaria

Florida International University, Miami, USA
V. Gaultney, L.M. Lebolo, S. Linn, P. Markowitz, G. Martinez, J.L. Rodriguez

Florida State University, Tallahassee, USA
T. Adams, A. Askew, J. Bochenek, J. Chen, B. Diamond, S.V. Gleyzer, J. Haas, S. Hagopian, V. Hagopian, M. Jenkins, K.F. Johnson, H. Prosper, L. Quertenmont, S. Sekmen, V. Veeraraghavan

Florida Institute of Technology, Melbourne, USA
M.M. Baarmand, B. Dorney, S. Guragain, M. Hohlmann, H. Kalakhety, R. Ralich, I. Vodopiyanov

University of Illinois at Chicago (UIC), Chicago, USA
M.R. Adams, I.M. Anghel, L. Apanasevich, Y. Bai, V.E. Bazterra, R.R. Betts, J. Callner, R. Cavanaugh, C. Dragoiu, L. Gauthier, C.E. Gerber, D.J. Hofman, S. Khalatyan, G.J. Kunde[47], F. Lacroix, M. Malek, C. O'Brien, C. Silkworth, C. Silvestre, A. Smoron, D. Strom, N. Varelas

The University of Iowa, Iowa City, USA
U. Akgun, E.A. Albayrak, B. Bilki, W. Clarida, F. Duru, C.K. Lae, E. McCliment, J.-P. Merlo, H. Mermerkaya[48], A. Mestvirishvili, A. Moeller, J. Nachtman, C.R. Newsom, E. Norbeck, J. Olson, Y. Onel, F. Ozok, S. Sen, J. Wetzel, T. Yetkin, K. Yi

Johns Hopkins University, Baltimore, USA
B.A. Barnett, B. Blumenfeld, A. Bonato, C. Eskew, D. Fehling, G. Giurgiu, A.V. Gritsan, Z.J. Guo, G. Hu, P. Maksimovic, S. Rappoccio, M. Swartz, N.V. Tran, A. Whitbeck

The University of Kansas, Lawrence, USA
P. Baringer, A. Bean, G. Benelli, O. Grachov, R.P. Kenny Iii, M. Murray, D. Noonan, S. Sanders, J.S. Wood, V. Zhukova

Kansas State University, Manhattan, USA
A.F. Barfuss, T. Bolton, I. Chakaberia, A. Ivanov, S. Khalil, M. Makouski, Y. Maravin, S. Shrestha, I. Svintradze, Z. Wan

Lawrence Livermore National Laboratory, Livermore, USA
J. Gronberg, D. Lange, D. Wright

University of Maryland, College Park, USA
A. Baden, M. Boutemeur, S.C. Eno, D. Ferencek, J.A. Gomez, N.J. Hadley, R.G. Kellogg, M. Kirn, Y. Lu, A.C. Mignerey, K. Rossato, P. Rumerio, F. Santanastasio, A. Skuja, J. Temple, M.B. Tonjes, S.C. Tonwar, E. Twedt

Massachusetts Institute of Technology, Cambridge, USA
B. Alver, G. Bauer, J. Bendavid, W. Busza, E. Butz, I.A. Cali, M. Chan, V. Dutta, P. Everaerts, G. Gomez Ceballos, M. Goncharov, K.A. Hahn, P. Harris, Y. Kim, M. Klute, Y.-J. Lee, W. Li, C. Loizides, P.D. Luckey, T. Ma, S. Nahn, C. Paus, D. Ralph, C. Roland, G. Roland, M. Rudolph, G.S.F. Stephans, F. Stöckli, K. Sumorok, K. Sung, D. Velicanu, E.A. Wenger, R. Wolf, S. Xie, M. Yang, Y. Yilmaz, A.S. Yoon, M. Zanetti

University of Minnesota, Minneapolis, USA
S.I. Cooper, P. Cushman, B. Dahmes, A. De Benedetti, P.R. Dudero, G. Franzoni, A. Gude, J. Haupt, K. Klapoetke, Y. Kubota, J. Mans, N. Pastika, V. Rekovic, R. Rusack, M. Sasseville, A. Singovsky, N. Tambe

University of Mississippi, University, USA
L.M. Cremaldi, R. Godang, R. Kroeger, L. Perera, R. Rahmat, D.A. Sanders, D. Summers

University of Nebraska-Lincoln, Lincoln, USA
K. Bloom, S. Bose, J. Butt, D.R. Claes, A. Dominguez, M. Eads, M. Gregoire, J. Keller, T. Kelly, I. Kravchenko, J. Lazo-Flores, H. Malbouisson, S. Malik, G.R. Snow

State University of New York at Buffalo, Buffalo, USA
U. Baur, A. Godshalk, I. Iashvili, S. Jain, A. Kharchilava, A. Kumar, S.P. Shipkowski, K. Smith, J. Zennamo

Northeastern University, Boston, USA
G. Alverson, E. Barberis, D. Baumgartel, O. Boeriu, M. Chasco, S. Reucroft, J. Swain, D. Trocino, D. Wood, J. Zhang

Northwestern University, Evanston, USA
A. Anastassov, A. Kubik, N. Odell, R.A. Ofierzynski, B. Pollack, A. Pozdnyakov, M. Schmitt, S. Stoynev, M. Velasco, S. Won

University of Notre Dame, Notre Dame, USA
L. Antonelli, D. Berry, A. Brinkerhoff, M. Hildreth, C. Jessop, D.J. Karmgard, J. Kolb, T. Kolberg, K. Lannon, W. Luo, S. Lynch, N. Marinelli, D.M. Morse, T. Pearson, R. Ruchti, J. Slaunwhite, N. Valls, M. Wayne, J. Ziegler

The Ohio State University, Columbus, USA
B. Bylsma, L.S. Durkin, J. Gu, C. Hill, P. Killewald, K. Kotov, T.Y. Ling, M. Rodenburg, G. Williams

Princeton University, Princeton, USA
N. Adam, E. Berry, P. Elmer, D. Gerbaudo, V. Halyo, P. Hebda, A. Hunt, J. Jones, E. Laird, D. Lopes Pegna, D. Marlow, T. Medvedeva, M. Mooney, J. Olsen, P. Piroué, X. Quan, B. Safdi, H. Saka, D. Stickland, C. Tully, J.S. Werner, A. Zuranski

University of Puerto Rico, Mayaguez, USA
J.G. Acosta, X.T. Huang, A. Lopez, H. Mendez, S. Oliveros, J.E. Ramirez Vargas, A. Zatserklyaniy

Purdue University, West Lafayette, USA
E. Alagoz, V.E. Barnes, G. Bolla, L. Borrello, D. Bortoletto, M. De Mattia, A. Everett, A.F. Garfinkel, L. Gutay, Z. Hu, M. Jones, O. Koybasi, M. Kress, A.T. Laasanen, N. Leonardo, C. Liu, V. Maroussov, P. Merkel, D.H. Miller, N. Neumeister, I. Shipsey, D. Silvers, A. Svyatkovskiy, H.D. Yoo, J. Zablocki, Y. Zheng

Purdue University Calumet, Hammond, USA
P. Jindal, N. Parashar

Rice University, Houston, USA
C. Boulahouache, K.M. Ecklund, F.J.M. Geurts, B.P. Padley, R. Redjimi, J. Roberts, J. Zabel

University of Rochester, Rochester, USA
B. Betchart, A. Bodek, Y.S. Chung, R. Covarelli, P. de Barbaro, R. Demina, Y. Eshaq, H. Flacher, A. Garcia-Bellido, P. Goldenzweig, Y. Gotra, J. Han, A. Harel, D.C. Miner, D. Orbaker, G. Petrillo, W. Sakumoto, D. Vishnevskiy, M. Zielinski

The Rockefeller University, New York, USA
A. Bhatti, R. Ciesielski, L. Demortier, K. Goulianos, G. Lungu, S. Malik, C. Mesropian

Rutgers, the State University of New Jersey, Piscataway, USA
O. Atramentov, A. Barker, D. Duggan, Y. Gershtein, R. Gray, E. Halkiadakis, D. Hidas, D. Hits, A. Lath, S. Panwalkar, R. Patel, K. Rose, S. Schnetzer, S. Somalwar, R. Stone, S. Thomas

University of Tennessee, Knoxville, USA
G. Cerizza, M. Hollingsworth, S. Spanier, Z.C. Yang, A. York

Texas A&M University, College Station, USA
R. Eusebi, W. Flanagan, J. Gilmore, A. Gurrola, T. Kamon, V. Khotilovich, R. Montalvo, I. Osipenkov, Y. Pakhotin, J. Pivarski, A. Safonov, S. Sengupta, A. Tatarinov, D. Toback, M. Weinberger

Texas Tech University, Lubbock, USA
N. Akchurin, C. Bardak, J. Damgov, C. Jeong, K. Kovitanggoon, S.W. Lee, T. Libeiro, P. Mane, Y. Roh, A. Sill, I. Volobouev, R. Wigmans, E. Yazgan

Vanderbilt University, Nashville, USA
E. Appelt, E. Brownson, D. Engh, C. Florez, W. Gabella, M. Issah, W. Johns, P. Kurt, C. Maguire, A. Melo, P. Sheldon, B. Snook, S. Tuo, J. Velkovska

University of Virginia, Charlottesville, USA
M.W. Arenton, M. Balazs, S. Boutle, B. Cox, B. Francis, J. Goodell, R. Hirosky, A. Ledovskoy, C. Lin, C. Neu, R. Yohay

Wayne State University, Detroit, USA
S. Gollapinni, R. Harr, P.E. Karchin, P. Lamichhane, M. Mattson, C. Milstène, A. Sakharov

University of Wisconsin, Madison, USA
M. Anderson, M. Bachtis, J.N. Bellinger, D. Carlsmith, S. Dasu, J. Efron, L. Gray, K.S. Grogg, M. Grothe, R. Hall-Wilton, M. Herndon, A. Hervé, P. Klabbers, J. Klukas, A. Lanaro, C. Lazaridis, J. Leonard, R. Loveless, A. Mohapatra, F. Palmonari, D. Reeder, I. Ross, A. Savin, W.H. Smith, J. Swanson, M. Weinberg

†: Deceased
1: Also at CERN, European Organization for Nuclear Research, Geneva, Switzerland
2: Also at Universidade Federal do ABC, Santo Andre, Brazil
3: Also at Laboratoire Leprince-Ringuet, Ecole Polytechnique, IN2P3-CNRS, Palaiseau, France
4: Also at Suez Canal University, Suez, Egypt
5: Also at British University, Cairo, Egypt
6: Also at Fayoum University, El-Fayoum, Egypt
7: Also at Soltan Institute for Nuclear Studies, Warsaw, Poland
8: Also at Massachusetts Institute of Technology, Cambridge, USA
9: Also at Université de Haute-Alsace, Mulhouse, France
10: Also at Brandenburg University of Technology, Cottbus, Germany
11: Also at Moscow State University, Moscow, Russia
12: Also at Institute of Nuclear Research ATOMKI, Debrecen, Hungary
13: Also at Eötvös Loránd University, Budapest, Hungary
14: Also at Tata Institute of Fundamental Research - HECR, Mumbai, India
15: Also at University of Visva-Bharati, Santiniketan, India
16: Also at Sharif University of Technology, Tehran, Iran
17: Also at Shiraz University, Shiraz, Iran
18: Also at Isfahan University of Technology, Isfahan, Iran
19: Also at Facoltà Ingegneria Università di Roma, Roma, Italy
20: Also at Università della Basilicata, Potenza, Italy
21: Also at Laboratori Nazionali di Legnaro dell' INFN, Legnaro, Italy
22: Also at Università degli studi di Siena, Siena, Italy
23: Also at California Institute of Technology, Pasadena, USA
24: Also at Faculty of Physics of University of Belgrade, Belgrade, Serbia
25: Also at University of California, Los Angeles, Los Angeles, USA
26: Also at University of Florida, Gainesville, USA
27: Also at Université de Genève, Geneva, Switzerland
28: Also at Scuola Normale e Sezione dell' INFN, Pisa, Italy
29: Also at University of Athens, Athens, Greece
30: Also at The University of Kansas, Lawrence, USA
31: Also at Institute for Theoretical and Experimental Physics, Moscow, Russia
32: Also at Paul Scherrer Institut, Villigen, Switzerland
33: Also at University of Belgrade, Faculty of Physics and Vinca Institute of Nuclear Sciences, Belgrade, Serbia
34: Also at Gaziosmanpasa University, Tokat, Turkey
35: Also at Adiyaman University, Adiyaman, Turkey
36: Also at The University of Iowa, Iowa City, USA
37: Also at Mersin University, Mersin, Turkey
38: Also at Izmir Institute of Technology, Izmir, Turkey
39: Also at Kafkas University, Kars, Turkey
40: Also at Suleyman Demirel University, Isparta, Turkey
41: Also at Ege University, Izmir, Turkey
42: Also at Rutherford Appleton Laboratory, Didcot, United Kingdom
43: Also at School of Physics and Astronomy, University of Southampton, Southampton, United Kingdom
44: Also at INFN Sezione di Perugia; Università di Perugia, Perugia, Italy
45: Also at Utah Valley University, Orem, USA
46: Also at Institute for Nuclear Research, Moscow, Russia

47: Also at Los Alamos National Laboratory, Los Alamos, USA
48: Also at Erzincan University, Erzincan, Turkey